Separable roles for RNAi in regulation of transposable elements and viability in the fission yeast *Schizosaccharomyces japonicus*

Elliott Chapman, Francesca Taglini[1] and Elizabeth H. Bayne[*]

Institute of Cell Biology, School of Biological Sciences, University of Edinburgh, Edinburgh, EH9 3FF, UK

[1]*Present address: MRC Human Genetics Unit, IGMM, University of Edinburgh, Edinburgh, EH4 2XU, UK; CRUK Edinburgh Centre, IGMM, University of Edinburgh, Edinburgh, EH4 2XU, UK*

[*]Correspondence: elizabeth.bayne@ed.ac.uk

ABSTRACT

RNA interference (RNAi) is a conserved mechanism of small RNA-mediated genome regulation commonly involved in suppression of transposable elements (TEs) through both post-transcriptional silencing, and transcriptional repression via heterochromatin assembly. The fission yeast *Schizosaccharomyces pombe* has been extensively utilised as a model for studying RNAi pathways. However, this species is somewhat atypical in that TEs are not major targets of RNAi, and instead small RNAs correspond primarily to non-coding pericentromeric repeat sequences, reflecting a specialised role for the pathway in promoting heterochromatin assembly in these regions. In contrast, in the related fission yeast *Schizosaccharomyces japonicus,* sequenced small RNAs correspond primarily to TEs. This suggests there may be fundamental differences in the operation of RNAi pathways in these two related species. To investigate these differences, we probed RNAi function in *S. japonicus*. Unexpectedly, and in contrast to *S. pombe*, we found that RNAi is essential in this species. Moreover, viability of RNAi mutants can be rescued by mutations implicated in enhanching RNAi-independent heterochromatin propagation. These rescued strains retain heterochromatic marks on TE sequences, but exhibit derepression of TEs at the post-transcriptional level. Our findings indicate that *S. japonicus* retains the ancestral role of RNAi in facilitating suppression of TEs via both post-transcriptional silencing and heterochromatin assembly, with specifically the heterochromatin pathway being essential for viability, likely due to a function in genome maintenance. The specialised role of RNAi in heterochromatin assembly in *S. pombe* appears to be a derived state that emerged after the divergence of *S. japonicus*.

INTRODUCTION

RNA interference is believed to have evolved as an ancient defence mechanism against invasive genetic elements such as viruses and TEs [1]. While canonical RNAi pathways operate via small RNA-guided post-transcriptional silencing of target RNAs, in some cases small RNAs can also direct chromatin modification to enact transcriptional repression [2]. Unusually, in the fission yeast *S. pombe,* such chromatin-level regulation appears to be the dominant function of RNAi, with the majority of small RNAs corresponding to specialised pericentromeric repeat sequences that are assembled into heterochromatin in an RNAi-dependent manner. Non-coding pericentromeric transcripts are processed by the Dicer nuclease Dcr1 to generate short interfering (si)RNAs that guide the Argonaute effector protein Ago1 to complementary nascent RNAs [3–6]. This promotes recruitment of the histone methyltransferase Clr4 [7,8], resulting in methylation of lysine 9 on histone H3 (H3K9me) and heterochromatin assembly at cognate chromatin [2,9,10]. Loss of pericentromeric heterochromatin impairs centromere function and hence strains lacking core RNAi components such as Dcr1 or Ago1, while viable, exhibit defects in chromosome segregation [11–13].

While the *S. pombe* RNAi system has become a paradigm for small RNA-directed chromatin modification, it appears atypical of RNAi pathways in general as it retains limited capacity for canonical post-transcriptional silencing [14–16], and plays a largely redundant role in TE control [17–20], with the small complement of endogenous retrotransposons instead regulated primarily by an alternative pathway involving CENP-B-like DNA binding proteins [21–23]. *S. japonicus* is another member of the fission yeast clade, estimated to have diverged from *S. pombe* around 220 million years ago [21]. Recent comparative analyses have revealed notable differences in genome organisation between the two species; in particular, *S. japonicus* appears to lack the specialised pericentromeric repeat sequences found in *S. pombe*, but has a much larger and more diverse complement of retrotransposons that appear to cluster at putative centromeric and telomeric loci [21,24]. Moreover, it appears there must also be key differences in mechanisms of retrotransposon regulation, since the CENP-B-like pathway that is active in *S. pombe* is absent in *S. japonicus* [21,25]. Interestingly however, retrotransposons in *S. japonicus* give rise to abundant siRNAs [21], and are enriched for heterochromatin-associated H3K9 methylation [21,24], suggesting that, in contrast to *S. pombe*, TE regulation may represent a major function of RNAi in *S. japonicus*.

In order to investigate functional divergence in RNAi pathways within the fission yeast clade, we set out to dissect the role of RNAi in *S. japonicus*. Unexpectedly, we were generally unable to recover viable deletion mutants for RNAi factors, indicating that unlike in *S. pombe*, RNAi

is essential for viability in *S. japonicus*. However, two viable *dcr1*$^+$ deletion strains were recovered, and analysis of these revealed that viability was linked to compensatory mutations promoting maintenance of H3K9 methylation independently of RNAi. While high levels of H3K9 methylation were maintained over retrotransposon loci in these strains, retrotransposons were nevertheless deregulated at the post-transcriptional level. Our findings reveal that *S. japonicus* retains the ancestral role of RNAi in regulating retrotransposons, and that the pathway serves dual functions: heterochromatin assembly over retrotransposons that is essential for viability, and post-transcriptional silencing of these elements that is dispensable.

RESULTS

To investigate RNAi function in *S. japonicus* we began by attempting to construct strains bearing deletions of genes encoding core RNAi factors including the sole Dicer and Argonaute proteins, Dcr1 and Ago1. Unexpectedly, with the exception of rare *dcr1*$^+$ mutant isolates (see below), we were unable to recover deletion mutants for any of these factors (Figure 1A and S1). We were also unable to recover strains deleted for the H3K9 methyltransferase Clr4. This was in contrast to deletion of genes known to not be required for the maintenance of heterochromatin (*pku70*$^+$*, pku80*$^+$ *and tri1*$^+$) [26], which could be achieved with high efficiency (Figure S1). Integration of epitope tags at RNAi gene loci could also be achieved with similar high efficiency (Figure S1), indicating that failure to recover RNAi deletion mutants does not reflect an intrinsic problem in targeting these loci. Rather, these observations suggest that, unlike in *S. pombe*, a functional RNAi pathway is essential for viability in *S. japonicus*. To verify this conclusion, we tested whether an RNAi gene could be deleted following genomic insertion of a second copy of the gene at an ectopic locus. Whereas we were unable to delete the *ago1*$^+$ gene in wild-type cells, deletions of endogenous *ago1*$^+$ were readily recovered in the presence of an ectopic copy of the gene that maintained Ago1 function (Figure 1A). Similar results were obtained for *dcr1*$^+$ and *clr4*$^+$. These findings strongly suggest that, in contrast to *S. pombe*, a functional RNAi pathway is usually required for cell viability in *S. japonicus*.

After extensive screening, we were able to recover two viable isolates bearing deletions of the *dcr1*$^+$ gene (hereafter denoted as *dcr1*Δ* *and dcr1*$\Delta^{\dagger}$ to indicate that these strains constitute rare survivors that may have acquired secondary mutations). The phenotypes of the two strains were indistinguishable, and for clarity only results for the *dcr1*Δ* strain are shown. Northern blot analysis indicated that retrotransposon-derived siRNAs were lost in the deletion strains, confirming the loss of function of Dcr1 (Figure 1B and S2). This was further confirmed by small RNA-seq analysis, which revealed populations of predominantly 23-24 nucleotide long siRNAs mapping to all ten families of Tj retrotransposon in wild-type cells that were lost

in the *dcr1*Δ* mutant (Figure 1C and S3). For some families of Tj element such as Tj7, discrete populations of small RNAs were detectable in the *dcr1*Δ* strain; however, these did not have the characteristic size distribution or 5'U bias associated with bona fide siRNAs (Figure 1C and S3)[27,28]. Moreover, whereas siRNAs are typically derived from both strands, these Dcr1-independent small RNAs corresponded almost exclusively to the sense strand of the retrotransposons, suggesting they are generated via an alternative RNA processing pathway (Figure 1C and 1D).

We reasoned that the increase in abundance of these alternative, sense-derived small RNA species in the *dcr1*Δ* mutant cells may reflect elevated retrotransposon mRNA levels. Consistent with this, RNA-seq analysis revealed increased accumulation of transcripts corresponding to centromere and telomere-clustered retrotransposons in *dcr1*Δ* compared to wild-type cells (Figure 2A). Indeed, TEs were found to constitute the majority of upregulated loci in *dcr1*Δ* cells (Figure 2B). Increased retrotransposon expression was also confirmed by RT-qPCR, with Tj7 showing the highest levels of transcript accumulation (Figure 2C and S4A). These observations indicate that, in contrast to *S. pombe* [18,19], Dcr1 plays a major role in regulating TE expression in *S. japonicus*.

To assess whether the increased retrotransposon expression is also associated with increased transposition, we assessed element copy number by qPCR in *dcr1*Δ* versus wild-type, parental cells. Nine out of ten retrotransposon families showed no increase in copy number in *dcr1*Δ* cells, suggesting that despite increased mRNA levels, these elements are not competent for transposition. On the other hand, Tj7, which showed the highest levels of transcript accumulation in the absence of functional Dcr1, increased in copy number by approximately 10-fold (Figure 2D and S4B). Coupled with the observation that Tj7 was the source of the vast majority of Dcr1-independent small RNAs in *dcr1*Δ* cells, (Figure 1B and 1C), this suggests that these alternative small RNA species may be associated with the retrotransposition process. Indeed, it is known that in the reverse transcription step of the mobilisation cycle, copying of single-stranded RNA into DNA is followed by RNase H-mediated cleavage of the RNA in the resulting DNA-RNA heteroduplex [29]. There is also evidence to suggest that RNase H cleavage sites are selected based on nucleotide preference within a defined sequence window [30–32]. Thus the observed Tj7-derived Dcr1-independent small RNA species are most likely RNase H cleavage products.

The RNA-seq analysis also revealed a number of genes up- and down-regulated in *dcr1*Δ* cells (Table S1). However, Gene Ontology analysis did not reveal any particular pathway enrichment amongst these genes, nor any other factors implicated in TE regulation. Interestingly, we also noted a number of previously unannotated genomic loci associated with

increased transcript and decreased siRNA levels in the *dcr1*Δ* cells, a signature otherwise characteristic of retrotransposon sequences. Indeed, analysis of these regions using the NCBI Conserved Domain Search tool [33] revealed that these loci largely comprised sequences encoding retrotransposon-specific protein domains (an example locus is shown in Figure 2E). Multiple-sequence alignment of these regions allowed us to identify 10 new retrotransposon families, that we have named Tj12 to Tj21 (Table S2). Phylogenetic analyses indicated that each of the new TEs falls into one of the two existing retrotransposon lineages in *S. japonicus* (Figure S5). The majority of TEs in the *S. japonicus* genome are densely clustered in putative centromeric and telomeric regions, and the newly identified retrotransposons tend to reside in windows of previously unannotated sequence within these regions, consistent with *S. japonicus* centromeres being composed almost exclusively of retrotransposon-derived sequences.

In *S. pombe*, the RNAi pathway mediates silencing primarily at the chromatin level, being required for proper maintenance of H3K9 methylation on pericentromeric repeats. To investigate whether silencing of retrotransposons is mediated via a similar mechanism in *S. japonicus*, we analysed H3K9 methylation by ChIP-seq. Unexpectedly, we found high levels of H3K9 methylation at retrotransposons in both wild-type and *dcr1*Δ* cells (Figure 3A). This was confirmed by ChIP-qPCR analyses, which showed no significant change in H3K9me2 levels at any retrotransposons in *dcr1*Δ* cells, suggesting that Dcr1 is not required to maintain H3K9me2 at TEs in these cells (Figure 3B and S6A). As a complementary approach to understanding whether retrotransposons are subject to Dcr1-dependent transcriptional regulation in *S. japonicus*, we also assessed RNA PolII association with retrotransposon loci by RNA PolII ChIP-qPCR. Consistent with the H3K9me ChIP results, we observed no change in RNA PolII occupancy at retrotransposons in *dcr1*Δ* cells (Figure 3C and S6B), indicating that increased transcript accumulation is not a result of increased transcription. Together these observations indicate that the elevated retrotransposons transcript levels observed in *dcr1*Δ* cells must be largely the result of loss of RNAi-mediated post-transcriptional silencing.

Since RNAi appears to be essential for viability in *S. japonicus*, and *dcr1*Δ strains were recovered only at very low frequency, we reasoned that some compensatory mutation(s) may be enabling viability in these rare *dcr1*Δ isolates. To search for such mutations, we undertook genome-resequencing of the two *dcr1* deletion strains. Sequence analysis revealed only a small number of mutations affecting protein-coding sequences, and from these a single strong candidate mutation was identified in each of the mutant strains. One strain (*dcr1*Δ*) carried a missense mutation (R77W) in the essential gene *mpe1*$^{+}$, which encodes the ortholog of budding yeast Mpe1, an E3 ubiquitin ligase that is a component of the cleavage and polyadenylation factor (CPF) complex [34,35] (Figure S7A). This is interesting since a recent

study implicated other components of the CPF complex in RNAi-independent heterochromatin assembly in *S. pombe* [36]. Hence one possibility is that the R77W mutation creates a gain of function allele of *mpe1*$^{+}$ that enhances H3K9 methylation in the absence of Dcr1. The other strain (*dcr1*Δ†) carried a frameshift mutation in the gene encoding Leo1, a component of the RNA polymerase-associated factor (PAF) complex (Figure S7B). The frameshift is predicted to introduce a premature stop codon at position 61, resulting in a severely truncated protein (Figure 4A). This mutation was particularly striking since we and others have recently shown that Leo1 is a negative regulator of heterochromatin that antagonises H3K9 methylation in *S. pombe* [37,38]. Thus loss of Leo1 function might be expected to facilitate maintenance of H3K9 methylation in the absence of RNAi.

To confirm whether loss of Leo1 function is sufficient to rescue the lethality associated with *dcr1*$^{+}$ deletion in *S. japonicus*, we generated a new *leo1*Δ strain, and then attempted to delete *dcr1*$^{+}$ in this background. Strikingly, isolates deleted for *dcr1*$^{+}$ could be recovered with high efficiency in the *leo1*Δ background (79% positive, Figure 4B). This efficiency was almost as high as when a second copy of *dcr1*$^{+}$ was present in the background (95% positive, Figure 1A). Thus absence of Leo1 can largely compensate for loss of Dcr1. To further investigate the mechanism of compensation, we next tested whether *leo1*$^{+}$ deletion can also suppress lethality associated with deletion of two other factors: the RNAi component Ago1, or the H3K9 methyltransferase Clr4. Interestingly, *ago1*Δ mutants could also be recovered with high efficiency in the *leo1*Δ background, suggesting that deletion of Leo1 can compensate for the loss of not just Dcr1, but the RNAi pathway more generally (Figure 4B). In contrast, we were unable to recover *clr4*$^{+}$ deletion mutants in the *leo1*Δ background. This indicates that compensation is dependent on H3K9 methylation. These observations are consistent with a model whereby lethality in RNAi mutants is associated with loss of H3K9 methylation, and deletion of *leo1*$^{+}$ restores viability by maintaining H3K9 methylation independently of RNAi. ChIP-qPCR analyses confirmed that H3K9me levels at retrotransposons remain high in *leo1*Δ *dcr1*Δ and *leo1*Δ *ago1*Δ double mutants, similar to wild-type cells (Figure 4C and S8C). In contrast, retrotransposons are still de-regulated in these mutants, as indicated by elevated transposon transcript levels and copy numbers relative to parental cells (Figure 4D-E and S8A-B). These findings indicate that RNAi targets retroelements at two distinct levels in *S. japonicus*: chromatin regulation through H3K9 methylation, and post-transcriptional regulation independent of H3K9 methylation. The maintenance of H3K9 methylation appears to be essential for viability, whilst post-transcriptional regulation of retroelements does not.

DISCUSSION

Suppression of TEs is an ancient and conserved role of small RNAs in eukaryotes. However, in the widely studied fission yeast model, *S. pombe*, the RNAi pathway has acquired a specialised role in heterochromatin assembly at specific repeat sequences and plays only a minor role in retrotransposon control [17–20]. Our observations now indicate that this specialisation occurred after the divergence from *S. japonicus*, the earliest branching member of the fission yeast clade, since an important function for RNAi in repressing active TEs is retained in *S. japonicus*. This repression occurs at both the transcriptional level, via deposition of repressive histone marks over retrotransposon sequences, and at the post transcriptional level, via Argonaute-mediated degradation of retrotransposon transcripts. This co-ordinated utilisation of transcriptional and post-transcriptional silencing in TE control is reminiscent of RNAi pathways in higher eukaryotes, and also has parallels with piRNA mediated repression of TEs in animals [39,40]. In these cases, whilst transcriptional silencing occurs in the nucleus, post-transcriptional transcript cleavage takes place in the cytoplasm, mediated by distinct Argonaute/PIWI family proteins [40]. As *S. japonicus* encodes only a single Argonaute, it will be interesting to investigate whether this protein forms distinct complexes for transcriptional and post-transcriptional repression, and whether these similarly function in discrete subcellular compartments.

An unexpected finding is that H3K9 methylation is essential for viability in *S. japonicus*. In mammals, depletion of RNAi factors Dicer or Ago2 leads to embryonic lethality [41,42], whilst disruption of Suv39h1/h2 (the mammalian homologues of Clr4) severely reduces viability during embryogenesis [43]. However, *S. pombe* strains lacking RNAi or heterochromatin factors are viable. In *S. pombe*, H3K9 methylation is required for binding of the HP1 protein Swi6 at pericentromeres, which in turn recruits cohesin to mediate tight sister chromatid cohesion and support proper interactions between kinetochores and the mitotic spindle [44–46]. Loss of Swi6 or H3K9 methylation causes loss of centromeric cohesion resulting in elevated rates of chromosome loss associated with increased incidence of lagging chromosomes on late anaphase spindles [44,47,48]. However, presence of lagging chromosomes is also associated with slowed spindle elongation, suggesting that *S. pombe* cells possess a mechanism that can sense a lagging chromosome and create extra time for it to reach the pole [49]. The nature of this mechanism is not understood, but if it is absent in *S. japonicus*, this could account for the much more severe defects in mutants lacking pericentromeric H3K9 methylation. In addition, while centromeric cohesin is lost in *S. pombe* heterochromatin mutants, arm cohesin is unaffected, and it appears that residual arm cohesion can partially compensate for the loss of centromeric cohesion and maintain the fidelity of chromosome segregation at a level compatible with viability [44,50]. Therefore

another possibility is that in *S. japonicus*, arm cohesion alone may be less effective in supporting accurate chromosome segregation, such that loss of centromeric heterochromatin has more catastrophic effects. Future comparative analyses of the factors underlying the differential sensitivity to loss of heterochromatin in these yeasts may shed further light on the evolution of mechanisms supporting centromere function.

Whilst the centromeric regions in *S. pombe* comprise specialised repeat sequences, in *S. japonicus* centromeres are defined by arrays of retrotransposon sequence. This is reminiscent of arrangements seen in humans, where centromeres contain both retroviral elements and long-interspersed nuclear elements (LINEs) [51] and plants, where specific centromeric retrotransposons (CRs) have been defined that are targeted by RNAi [52]. Likewise, Drosophila centromeres are TE-rich [53,54], and processing of retrotransposon transcripts into siRNAs is required to maintain pericentromeric heterochromatin [55]. Thus in the utilisation of RNAi as a primary mechanism to regulate TEs, the centromeric clustering of these mobile elements, and their use as a platform for assembly of critical heterochromatin, *S. japonicus* has much in common with plants and animals, establishing it as an attractive model in which to study both RNAi and centromere function.

ACKNOWLEDGEMENTS

Thanks are due to the Oliferenko lab for strains and advice on *S. japonicus* transformation, to Hironori Niki for strains, and to Takeshi Urano for the H3K9me2 antibody. Thanks to Darren Obbard for advice on construction of phylogenetic trees. We are grateful to Alison Pidoux and Jo Strachan for advice and comments on the manuscript and to members of the Bayne lab for discussions. Total RNA and siRNA sequencing was carried out by Edinburgh Genomics, The University of Edinburgh. ChIP and genomic DNA sequencing was carried out by the Edinburgh Clinical Research Facility. Our work was supported by BBSRC PhD studentships to EC (1311387) and FT (1101397), and a MRC Career Development Award (G1000505) and Wellcome Trust Investigator Award (202771/Z/16/Z) to EHB.

AUTHOR CONTRIBUTIONS

EC, FT and EHB designed the study. FT initiated the experimental work; EC performed most of the experimental work and the bioinformatic analyses. EC and EHB co-wrote the manuscript; all authors edited the manuscript. EHB supervised the project and acquired funding.

DECLARATION OF INTERESTS

The authors declare no competing interests.

DATA AVAILABILITY

RNA-Seq, sRNA-Seq and ChIP-Seq datasets have been deposited in the Gene Expression Omnibus (GEO) under accession number GSE185665. Genomic DNA sequencing datasets have been deposited in the Sequence Read Archive (SRA) under accession number PRJNA770288.

REFERENCES

1. Obbard DJ, Gordon KHJ, Buck AH, Jiggins FM. The evolution of RNAi as a defence against viruses and transposable elements. Philosophical Transactions of the Royal Society B: Biological Sciences. 2009;364. doi:10.1098/rstb.2008.0168

2. Martienssen R, Moazed D. RNAi and Heterochromatin Assembly. Cold Spring Harbor Perspectives in Biology. 2015;7. doi:10.1101/cshperspect.a019323

3. Volpe TA, Kidner C, Hall IM, Teng G, Grewal SIS, Martienssen RA. Regulation of Heterochromatic Silencing and Histone H3 Lysine-9 Methylation by RNAi. Science. 2002;297. doi:10.1126/science.1074973

4. Verdel A, Jia S, Gerber S, Sugiyama T, Gygi S, Grewal SIS, et al. RNAi-Mediated Targeting of Heterochromatin by the RITS Complex. Science. 2004;303. doi:10.1126/science.1093686

5. Shimada Y, Mohn F, Bühler M. The RNA-induced transcriptional silencing complex targets chromatin exclusively via interacting with nascent transcripts. Genes & Development. 2016;30. doi:10.1101/gad.292599.116

6. Bühler M, Verdel A, Moazed D. Tethering RITS to a Nascent Transcript Initiates RNAi- and Heterochromatin-Dependent Gene Silencing. Cell. 2006;125. doi:10.1016/j.cell.2006.04.025

7. Zhang K, Mosch K, Fischle W, Grewal SIS. Roles of the Clr4 methyltransferase complex in nucleation, spreading and maintenance of heterochromatin. Nature Structural & Molecular Biology. 2008;15. doi:10.1038/nsmb.1406

8. Nakayama J -i., Rice JC, Strahl BD, Allis CD, Grewal SIS. Role of Histone H3 Lysine 9 Methylation in Epigenetic Control of Heterochromatin Assembly. Science. 2001;292. doi:10.1126/science.1060118

9. Allshire RC, Ekwall K. Epigenetic Regulation of Chromatin States in *Schizosaccharomyces pombe*. Cold Spring Harbor Perspectives in Biology. 2015;7. doi:10.1101/cshperspect.a018770

10. Grewal SI. RNAi-dependent formation of heterochromatin and its diverse functions. Current Opinion in Genetics & Development. 2010;20. doi:10.1016/j.gde.2010.02.003

11. Volpe T, Schramke V, Hamilton GL, White SA, Teng G, Martienssen RA, et al. RNA interference is required for normal centromere function in fission yeast. Chromosome Research. 2003;11. doi:10.1023/A:1022815931524

12. Hall IM, Noma K -i., Grewal SIS. RNA interference machinery regulates chromosome dynamics during mitosis and meiosis in fission yeast. Proceedings of the National Academy of Sciences. 2003;100. doi:10.1073/pnas.232688099

13. Provost P, Silverstein RA, Dishart D, Walfridsson J, Djupedal I, Kniola B, et al. Dicer is required for chromosome segregation and gene silencing in fission yeast cells. Proceedings of the National Academy of Sciences. 2002;99. doi:10.1073/pnas.212633199

14. Simmer F, Buscaino A, Kos-Braun IC, Kagansky A, Boukaba A, Urano T, et al. Hairpin RNA induces secondary small interfering RNA synthesis and silencing in *trans* in fission yeast. EMBO reports. 2010;11. doi:10.1038/embor.2009.273

15. Iida T, Kawaguchi R, Nakayama J. Conserved Ribonuclease, Eri1, Negatively Regulates Heterochromatin Assembly in Fission Yeast. Current Biology. 2006;16. doi:10.1016/j.cub.2006.05.061

16. Sigova A, Rhind N, Zamore PD. A single Argonaute protein mediates both transcriptional and posttranscriptional silencing in Schizosaccharomyces pombe. Genes & Development. 2004;18. doi:10.1101/gad.1218004

17. Cam HP, Sugiyama T, Chen ES, Chen X, FitzGerald PC, Grewal SIS. Comprehensive analysis of heterochromatin- and RNAi-mediated epigenetic control of the fission yeast genome. Nature Genetics. 2005;37. doi:10.1038/ng1602

18. Hansen KR, Burns G, Mata J, Volpe TA, Martienssen RA, Bähler J, et al. Global Effects on Gene Expression in Fission Yeast by Silencing and RNA Interference Machineries. Molecular and Cellular Biology. 2005;25. doi:10.1128/MCB.25.2.590-601.2005

19. Woolcock KJ, Gaidatzis D, Punga T, Bühler M. Dicer associates with chromatin to repress genome activity in Schizosaccharomyces pombe. Nature Structural & Molecular Biology. 2011;18. doi:10.1038/nsmb.1935

20. Yamanaka S, Mehta S, Reyes-Turcu FE, Zhuang F, Fuchs RT, Rong Y, et al. RNAi triggered by specialized machinery silences developmental genes and retrotransposons. Nature. 2013;493. doi:10.1038/nature11716

21. Rhind N, Chen Z, Yassour M, Thompson DA, Haas BJ, Habib N, et al. Comparative Functional Genomics of the Fission Yeasts. Science. 2011;332. doi:10.1126/science.1203357

22. Cam HP, Noma K, Ebina H, Levin HL, Grewal SIS. Host genome surveillance for retrotransposons by transposon-derived proteins. Nature. 2008;451. doi:10.1038/nature06499

23. Lorenz DR, Mikheyeva I v., Johansen P, Meyer L, Berg A, Grewal SIS, et al. CENP-B Cooperates with Set1 in Bidirectional Transcriptional Silencing and Genome Organization of Retrotransposons. Molecular and Cellular Biology. 2012;32. doi:10.1128/MCB.00395-12

24. Tong P, Pidoux AL, Toda NRT, Ard R, Berger H, Shukla M, et al. Interspecies conservation of organisation and function between nonhomologous regional centromeres. Nature Communications. 2019;10. doi:10.1038/s41467-019-09824-4

25. Upadhyay U, Srivastava S, Khatri I, Nanda JS, Subramanian S, Arora A, et al. Ablation of RNA interference and retrotransposons accompany acquisition and evolution of transposases to heterochromatin protein CENPB. Molecular Biology of the Cell. 2017;28. doi:10.1091/mbc.e16-07-0485

26. Marasovic M, Zocco M, Halic M. Argonaute and Triman Generate Dicer-Independent priRNAs and Mature siRNAs to Initiate Heterochromatin Formation. Molecular Cell. 2013;52. doi:10.1016/j.molcel.2013.08.046

27. Djupedal I, Kos-Braun IC, Mosher RA, Söderholm N, Simmer F, Hardcastle TJ, et al. Analysis of small RNA in fission yeast; centromeric siRNAs are potentially generated through a structured RNA. The EMBO Journal. 2009;28. doi:10.1038/emboj.2009.351

28. Bühler M, Spies N, Bartel DP, Moazed D. TRAMP-mediated RNA surveillance prevents spurious entry of RNAs into the *Schizosaccharomyces pombe* siRNA pathway. Nature Structural & Molecular Biology. 2008;15. doi:10.1038/nsmb.1481

29. Hughes SH. Reverse Transcription of Retroviruses and LTR Retrotransposons. Microbiology Spectrum. 2015;3. doi:10.1128/microbiolspec.MDNA3-0027-2014

30. Schultz SJ, Champoux JJ. RNase H activity: Structure, specificity, and function in reverse transcription. Virus Research. 2008;134. doi:10.1016/j.virusres.2007.12.007

31. Schultz SJ, Zhang M, Champoux JJ. Preferred Sequences within a Defined Cleavage Window Specify DNA 3′ End-directed Cleavages by Retroviral RNases H. Journal of Biological Chemistry. 2009;284. doi:10.1074/jbc.M109.043158

32. Schultz SJ, Zhang M, Champoux JJ. Sequence, Distance, and Accessibility Are Determinants of 5′-End-directed Cleavages by Retroviral RNases H. Journal of Biological Chemistry. 2006;281. doi:10.1074/jbc.M510504200

33. Lu S, Wang J, Chitsaz F, Derbyshire MK, Geer RC, Gonzales NR, et al. CDD/SPARCLE: the conserved domain database in 2020. Nucleic Acids Research. 2020;48. doi:10.1093/nar/gkz991

34. Lee SD, Moore CL. Efficient mRNA Polyadenylation Requires a Ubiquitin-Like Domain, a Zinc Knuckle, and a RING Finger Domain, All Contained in the Mpe1 Protein. Molecular and Cellular Biology. 2014;34. doi:10.1128/MCB.00077-14

35. Vo LTA, Minet M, Schmitter J-M, Lacroute F, Wyers F. Mpe1, a Zinc Knuckle Protein, Is an Essential Component of Yeast Cleavage and Polyadenylation Factor Required for the Cleavage and Polyadenylation of mRNA. Molecular and Cellular Biology. 2001;21. doi:10.1128/MCB.21.24.8346-8356.2001

36. Lee SY, Hung S, Esnault C, Pathak R, Johnson KR, Bankole O, et al. Dense Transposon Integration Reveals Essential Cleavage and Polyadenylation Factors Promote Heterochromatin Formation. Cell Reports. 2020;30. doi:10.1016/j.celrep.2020.01.094

37. Verrier L, Taglini F, Barrales RR, Webb S, Urano T, Braun S, et al. Global regulation of heterochromatin spreading by Leo1. Open Biology. 2015;5. doi:10.1098/rsob.150045

38. Sadeghi L, Prasad P, Ekwall K, Cohen A, Svensson JP. The Paf1 complex factors Leo1 and Paf1 promote local histone turnover to modulate chromatin states in fission yeast. EMBO reports. 2015;16. doi:10.15252/embr.201541214

39. Gutbrod MJ, Martienssen RA. Conserved chromosomal functions of RNA interference. Nature Reviews Genetics. 2020;21. doi:10.1038/s41576-019-0203-6

40. Onishi R, Yamanaka S, Siomi MC. piRNA- and siRNA-mediated transcriptional repression in *Drosophila* , mice, and yeast: new insights and biodiversity. EMBO reports. 2021. doi:10.15252/embr.202153062

41. Bernstein E, Kim SY, Carmell MA, Murchison EP, Alcorn H, Li MZ, et al. Dicer is essential for mouse development. Nature Genetics. 2003;35. doi:10.1038/ng1253

42. Liu J, Carmell MA, Rivas F v, Marsden CG, Thomson JM, Song J-J, et al. Argonaute2 is the catalytic engine of mammalian RNAi. Science (New York, NY). 2004;305. doi:10.1126/science.1102513

43. Peters AHFM, O'Carroll D, Scherthan H, Mechtler K, Sauer S, Schöfer C, et al. Loss of the Suv39h Histone Methyltransferases Impairs Mammalian Heterochromatin and Genome Stability. Cell. 2001;107. doi:10.1016/S0092-8674(01)00542-6

44. Bernard P, Maure JF, Partridge JF, Genier S, Javerzat JP, Allshire RC. Requirement of Heterochromatin for Cohesion at Centromeres. Science. 2001;294. doi:10.1126/science.1064027

45. Nonaka N, Kitajima T, Yokobayashi S, Xiao G, Yamamoto M, Grewal SIS, et al. Recruitment of cohesin to heterochromatic regions by Swi6/HP1 in fission yeast. Nature Cell Biology. 2002;4. doi:10.1038/ncb739

46. Bannister AJ, Zegerman P, Partridge JF, Miska EA, Thomas JO, Allshire RC, et al. Selective recognition of methylated lysine 9 on histone H3 by the HP1 chromo domain. Nature. 2001;410. doi:10.1038/35065138

47. Ekwall K, Javerzat J, Lorentz A, Schmidt H, Cranston G, Allshire R. The chromodomain protein Swi6: a key component at fission yeast centromeres. Science. 1995;269. doi:10.1126/science.7660126

48. Allshire RC, Nimmo ER, Ekwall K, Javerzat JP, Cranston G. Mutations derepressing silent centromeric domains in fission yeast disrupt chromosome segregation. Genes & Development. 1995;9. doi:10.1101/gad.9.2.218

49. Pidoux AL, Uzawa S, Perry PE, Cande WZ, Allshire RC. Live analysis of lagging chromosomes during anaphase and their effect on spindle elongation rate in fission yeast. Journal of Cell Science. 2000;113. doi:10.1242/jcs.113.23.4177

50. Pidoux AL, Allshire RC. The role of heterochromatin in centromere function. Philosophical Transactions of the Royal Society B: Biological Sciences. 2005;360. doi:10.1098/rstb.2004.1611

51. Smurova K, de Wulf P. Centromere and Pericentromere Transcription: Roles and Regulation … in Sickness and in Health. Frontiers in Genetics. 2018;9. doi:10.3389/fgene.2018.00674

52. Neumann P, Navrátilová A, Koblížková A, Kejnovský E, Hřibová E, Hobza R, et al. Plant centromeric retrotransposons: a structural and cytogenetic perspective. Mobile DNA. 2011;2. doi:10.1186/1759-8753-2-4

53. Hoskins RA, Carlson JW, Kennedy C, Acevedo D, Evans-Holm M, Frise E, et al. Sequence Finishing and Mapping of Drosophila melanogaster Heterochromatin. Science. 2007;316. doi:10.1126/science.1139816

54. Chang C-H, Chavan A, Palladino J, Wei X, Martins NMC, Santinello B, et al. Islands of retroelements are major components of Drosophila centromeres. PLOS Biology. 2019;17. doi:10.1371/journal.pbio.3000241

55. Hao Y, Wang D, Wu S, Li X, Shao C, Zhang P, et al. Active retrotransposons help maintain pericentromeric heterochromatin required for faithful cell division. Genome Research. 2020;30. doi:10.1101/gr.256131.119

56. Sabatinos SA, Forsburg SL. Molecular Genetics of *Schizosaccharomyces pombe*. Methods in Enzymology. 2010. doi:10.1016/S0076-6879(10)70032-X

57. Nozaki S, Furuya K, Niki H. The Ras1-Cdc42 pathway is involved in hyphal development of *Schizosaccharomyces japonicus*. FEMS Yeast Research. 2018;18. doi:10.1093/femsyr/foy031

58. Furuya K, Niki H. The DNA Damage Checkpoint Regulates a Transition between Yeast and Hyphal Growth in *Schizosaccharomyces japonicus*. Molecular and Cellular Biology. 2010;30. doi:10.1128/MCB.00049-10

59. Pieper GH, Sprenger S, Teis D, Oliferenko S. ESCRT-III/Vps4 Controls Heterochromatin-Nuclear Envelope Attachments. Developmental Cell. 2020;53. doi:10.1016/j.devcel.2020.01.028

60. Noguchi C, Garabedian M v., Malik M, Noguchi E. A vector system for genomic FLAG epitope-tagging in *Schizosaccharomyces pombe*. Biotechnology Journal. 2008;3. doi:10.1002/biot.200800140

61. Aoki K, Niki H. Transformation of *Schizosaccharomyces japonicus*. Cold Spring Harbor Protocols. 2017;2017. doi:10.1101/pdb.prot091850

62. Pall GS, Hamilton AJ. Improved northern blot method for enhanced detection of small RNA. Nature Protocols. 2008;3. doi:10.1038/nprot.2008.67

63. Afgan E, Baker D, Batut B, van den Beek M, Bouvier D, Čech M, et al. The Galaxy platform for accessible, reproducible and collaborative biomedical analyses: 2018 update. Nucleic Acids Research. 2018;46. doi:10.1093/nar/gky379

64. Krueger F, James F, Ewels P, Afyounian E, Schuster-Boeckler B. TrimGalore. 23 Jul 2021 [cited 14 Oct 2021]. doi:10.5281/ZENODO.5127899

65. Dobin A, Davis CA, Schlesinger F, Drenkow J, Zaleski C, Jha S, et al. STAR: ultrafast universal RNA-seq aligner. Bioinformatics. 2013;29. doi:10.1093/bioinformatics/bts635

66. Liao Y, Smyth GK, Shi W. featureCounts: an efficient general purpose program for assigning sequence reads to genomic features. Bioinformatics. 2014;30. doi:10.1093/bioinformatics/btt656

67. Teissandier A, Servant N, Barillot E, Bourc'his D. Tools and best practices for retrotransposon analysis using high-throughput sequencing data. Mobile DNA. 2019;10. doi:10.1186/s13100-019-0192-1

68. Robinson MD, McCarthy DJ, Smyth GK. edgeR: a Bioconductor package for differential expression analysis of digital gene expression data. Bioinformatics. 2010;26. doi:10.1093/bioinformatics/btp616

69. Ramírez F, Ryan DP, Grüning B, Bhardwaj V, Kilpert F, Richter AS, et al. deepTools2: a next generation web server for deep-sequencing data analysis. Nucleic Acids Research. 2016;44. doi:10.1093/nar/gkw257

70. Young MD, Wakefield MJ, Smyth GK, Oshlack A. Gene ontology analysis for RNA-seq: accounting for selection bias. Genome Biology. 2010;11. doi:10.1186/gb-2010-11-2-r14

71. Langmead B, Salzberg SL. Fast gapped-read alignment with Bowtie 2. Nature Methods. 2012;9. doi:10.1038/nmeth.1923

72. Webster CL, Waldron FM, Robertson S, Crowson D, Ferrari G, Quintana JF, et al. The Discovery, Distribution, and Evolution of Viruses Associated with Drosophila melanogaster. PLOS Biology. 2015;13. doi:10.1371/journal.pbio.1002210

73. Thompson JD, Higgins DG, Gibson TJ. CLUSTAL W: improving the sensitivity of progressive multiple sequence alignment through sequence weighting, position-specific gap penalties and weight matrix choice. Nucleic Acids Research. 1994;22. doi:10.1093/nar/22.22.4673

74. Minh BQ, Schmidt HA, Chernomor O, Schrempf D, Woodhams MD, von Haeseler A, et al. IQ-TREE 2: New Models and Efficient Methods for Phylogenetic Inference in the Genomic Era. Molecular Biology and Evolution. 2020;37. doi:10.1093/molbev/msaa015

75. Rambaut A. FigTree. Tree Figure Drawing Tool. 2009 [cited 21 Oct 2021]. Available: http://tree.bio.ed.ac.uk/software/figtree/

76. Nakagawachi T, Soejima H, Urano T, Zhao W, Higashimoto K, Satoh Y, et al. Silencing effect of CpG island hypermethylation and histone modifications on O6-methylguanine-DNA methyltransferase (MGMT) gene expression in human cancer. Oncogene. 2003;22. doi:10.1038/sj.onc.1207183

77. Seemann T. snippy: fast bacterial variant calling from NGS reads. 2015 [cited 14 Oct 2021]. Available: https://github.com/tseemann/snippy

78. Furuya K, Niki H. Isolation of heterothallic haploid and auxotrophic mutants of *Schizosaccharomyces japonicus*. Yeast. 2009;26. doi:10.1002/yea.1662

79. Furuya K, Niki H. Construction of diploid zygotes by interallelic complementation of *ade6* in *Schizosaccharomyces japonicus*. Yeast. 2011;28. doi:10.1002/yea.1898

80. Hentges P, van Driessche B, Tafforeau L, Vandenhaute J, Carr AM. Three novel antibiotic marker cassettes for gene disruption and marker switching in *Schizosaccharomyces pombe*. Yeast. 2005;22. doi:10.1002/yea.1291

81. Maundrell K. Thiamine-repressible expression vectors pREP and pRIP for fission yeast. Gene. 1993;123. doi:10.1016/0378-1119(93)90551-D

MATERIALS AND METHODS

Strains, media, and culture conditions

S. japonicus strains used in this study are listed in Supplementary Table S3. Cells were grown in rich liquid YES media [56], or plated onto rich solid YES or minimal solid PMG media at 32°C unless otherwise stated.

Strain construction

As genomic integration of exogenous DNA into *S. japonicus* requires long flanking homologies [57], fragments for homologous recombination were either amplified from purpose-built vectors or were constructed using overlap fusion PCR. For the deletion of *ago1*$^+$*, clr4*$^+$ and *dcr1*$^+$*,* vectors were built by restriction endonuclease cloning, using pFA6a-natMX6 as a backbone (all plasmids used in this study are listed in Supplementary Table S4). For the *ago1Δ* and *clr4Δ* constructs, flanking homologies were generated by PCR amplification of a 1kb region upstream of the target gene start codon and a 1kb region downstream of the target gene stop codon, these were then subsequently restriction cloned into pFA6a-natMX6, either side of the natMX6 cassette. For the *dcr1Δ* constructs, the upstream flanking homology was generated in the same way as for *ago1Δ* and *clr4Δ*, whilst two versions of the downstream flanking homology were constructed, both of which delete a portion of the *dcr1*$^+$ open reading frame without interfering with any genes coded on the opposite strand. The first deletes the initial 108bp of the coding sequence and was named *dcr1Δ*^{dis}, whilst the second deletes a larger 2520bp portion and was termed *dcr1Δ*^{del}*.* These flanking homologies were also restriction cloned into pFA6a-natMX6, either side of the natMX6 cassette. The resulting four vectors: pFA6a-*dcr1Δ*^{dis}-natMX6, pFA6a-*dcr1Δ*^{del}-natMX6, pFA6a-*ago1Δ*-natMX6 and pFA6a-*clr4Δ*-natMX6 were used as templates for PCR. Deletion constructs for *arb1*$^+$*, arb2*$^+$*, chp1*$^+$*, rdp1*$^+$*, rik1*$^+$*, stc1*$^+$*, tri1*$^+$*, pku70*$^+$ *and pku80*$^+$ were constructed using overlap fusion PCR of three fragments generated by PCR amplification of a 1kb region upstream of the target gene start codon, the HindIII *ura4*$^+$ fragment from *S. pombe,* and a 1kb region downstream of the target gene stop codon. For deletion of *leo1*$^+$ a vector was built using the NEBuilder HiFi kit, whereby a 1kb upstream homology arm, the HindIII *ura4*$^+$ fragment from *S. pombe* and a 1kb downstream homology arm were cloned into a pFA6a backbone. The resulting vector pFA6a-*leo1Δ-ura4* was used as a template for PCR. In order to introduce ectopic gene copies at the *nmt1*$^+$ locus, an *S. japonicus* version of the pREP1 vector was first constructed, whereby the *S. pombe nmt1*$^+$ promoter and terminator were swapped for the corresponding *S. japonicus* versions [58]. The open reading frames of *ago1*$^+$, *clr4*$^+$ and *dcr1*$^+$ were subsequently cloned between the *nmt1*$^+$ promoter and terminator, and the resultant plasmids (pREP1SJ-*ago1*$^+$,

pREP1SJ-*clr4*$^+$, pREP1SJ-*dcr1*$^+$) were used as templates for PCR. For C-terminal tagging of *chp1*$^+$, *rik1*$^+$ and *stc1*$^+$, 1kb fragments corresponding to the region immediately upstream of the target gene stop codon, and the region downstream of the target gene 3'UTR, were PCR amplified and cloned into either pSO729 (eGFP) [59] or pFA6a-FLAG-natMX6 (5xFLAG) [60]. The resultant plasmids were linearised with NdeI for pFA6a-FLAG-NatMX6 or XhoI for pSO729 for use as linear transformation fragments. N-terminal tagging of *ago1*$^+$ was achieved using overlap fusion PCR of three fragments comprising a 1kb region upstream of the *ago1*$^+$ start codon, the kanMX6-P3nmt1-NFLAG module from pFA6a-kanMX6-P3nmt1-NFLAG [60], and the first 1kb of the *ago1*$^+$ coding sequence. Transformation of *S. japonicus* was performed by electroporation [61], and cells were selected on the appropriate YES + antibiotic or PMG amino acid dropout plates.

RNA isolation

Total RNA was extracted from 2ml of cells at OD_{595} = 0.8-1.0 using the Masterpure Yeast RNA Purification Kit (Lucigen). Small RNAs were extracted by resuspending 50ml of pelleted cells at OD_{595} = 0.8-1.0 in 50 mM Tris–HCl pH 7.5, 10 mM EDTA pH 8, 100 mM NaCl, 1% SDS, and adding equal volumes of phenol:chloroform 5:1 and acid washed beads. Cells were lysed using a bead beater (Biospec products) for 2 x 2 min at 4°C. The soluble fraction was extracted with phenol/chloroform and long RNAs precipitated with 10% polyethylene glycol 8000 and 0.5 M NaCl on ice for 30 min. The supernatant was recovered and small RNAs precipitated with ethanol overnight at −20°C.

Northern blot

Northern analysis of small RNAs was performed as described previously [62]. Briefly, RNA samples were run on a 12% polyacrylamide gel, electrophoretically transferred onto Hybond-NX (Amersham) and crosslinked by incubation at 55°C for 2 hours with a 0.16 M carbodiimide, 1-ethyl-3-(3-dimethylaminopropyl) carbodiimide (EDC) solution. Membranes were probed with 5′ end radiolabelled oligonucleotides listed in Supplementary Table S5.

RT-qPCR

For RT-qPCR analysis, 1µg of total RNA was treated with TURBO DNase (Ambion) for 1 hour at 37°C, then reverse transcribed using random hexamers (Roche) and Superscript III reverse transcriptase (Invitrogen) according to the manufacturer's instructions. cDNA was quantified by qPCR using LightCycler 480 SYBR Green (Roche) and primers listed in Supplementary Table S5.

RNA-seq

Libraries were prepared using Illumina TruSeq stranded mRNA library preparation kit according to manufacturer's instructions, then pooled and sequenced paired-end on an Illumina HiSeq4000. Bioinformatic analysis was carried out using the Galaxy server [63]. Raw reads were filtered for quality and adapter using Trim Galore! (version 0.4.3.1) [64]. Trimmed reads were then aligned to the *S. japonicus* reference genome SJ5 (GCA_000149845.2) using STAR (version 2.7.2b) [65]. Read counts were obtained using featureCounts (version 1.6.4) [66] with settings -M –fraction [67], and differential gene expression then performed using edgeR (version 3.21.1) [68]. For visualisation, bedgraph coverage files were generated using bamCoverage (version 3.3.2.0.0) [69]. Gene Ontology (GO) and KEGG pathway analysis was performed using goseq (version 1.44.0) [70].

Small RNA-seq

Libraries were prepared using lllumina TruSeq small RNA library preparation kit according to manufacturer's instructions, then pooled and sequenced single-end on an Illumina HiSeq2500. Bioinformatic analysis was carried out using the Galaxy server [63], Raw reads were filtered for quality and adapter using Trim Galore! (version 0.4.3.1) [64]. Trimmed reads were then aligned to the *S. japonicus* reference genome SJ5 (GCA_000149845.2) using bowtie2 (version 2.3.4.3) [71]. For visualisation, bedgraph coverage files were generated using bamCoverage (version 3.3.2.0.0) [69]. Plots detailing the length, strand bias and first nucleotide preference of small RNAs mapping to transposable elements were created using a previously published custom R script [72].

Annotation of new retrotransposon families

Read coverage tracks for the mRNA-Seq and sRNA-Seq experiments were loaded into IGV alongside the latest SJ5 .gff file (Schizosaccharomyces_japonicus. GCA_000149845.2.51.gff3), updated to include the co-ordinates of the retrotransposons Tj1-Tj10, as previously specified [21]. Regions that did not have an annotation but exhibited lost or changed small RNA signals and increased mRNA coverage in the *dcr1Δ** mutant were manually identified. The NCBI Conserved Domain Search tool [33] was then used to search these regions for any sequences potentially coding for retrotransposon-associated protein domains (gag, protease, reverse transcriptatse, RNase, integrase, chromodomain). Where such domains were found, up- and downstream sequences were searched for direct repeats that could correspond to LTRs, which define retrotransposon borders and would indicate the presence of a full length TE. Any regions larger than 1kb that contained at least one retrotransposon-related protein motif were then searched against rest of the *S. japonicus*

reference genome SJ5 (GCA_000149845.2) to identify any additional copies. From this analysis, three previously unannotated full length retrotransposons, 79 partial retrotransposons, and 32 solo-LTRs were identified. Alignment of the newly identified reverse transcriptase, RNase H and integrase domain sequences with the corresponding domains from Tj1-10 using Clustal Omega revealed 10 novel retrotransposon families. We also identified the Tj11 element recently described by the Allshire lab [24]. The co-ordinates of the retrotransposons Tj1-21 are detailed in Supplementary Table 2.

Phylogenetic analysis of retrotransposons

In order to classify the newly discovered retrotransposons, the sequences of the reverse transcriptase, RNase and integrase domains were aligned to the corresponding domains from Tj1-10, as well as *S. pombe* Tf1 and Tf2 and *S. cerevisiae* Ty3 using ClustalW [73]. IQtree2 [74] was then used to build a single tree based on the three loci, with 1000 ultrafast bootstraps. IQtree2 selected TVM+F+R3 as the best-fitting base substitution model using the Bayesian Information Criterion (BIC). The resulting tree was opened and edited using FigTree [75] to display the bootstrapping values as node labels.

ChIP-qPCR

50ml of cells per IP were grown in YES to an OD_{595} of 0.8-1.0, and were fixed in 1% formaldehyde for 15 min at room temperature. Cells were lysed in 350µl of 50mM Hepes-KOH pH7.5, 140mM NaCl, 1mM EDTA, 1% (v/v) Triton X-100, 0.1%(w/v) sodium deoxycholate, 1x PMSF, 1x yeast protease inhibitors (Roche) using a bead beater (Biospec products) for 2 x 2 min at 4°C. Sonication was performed using a Bioruptor Twin (Diagenode) for a total of 20 min (30 sec on/30 sec off on 'high' power). Samples were pre-cleared using 25µl Protein G Agarose beads, before lysates were incubated overnight at 4°C, with 1µl per IP of anti-H3K9me2 (mAb 5.1.1 [76]), 2µl per IP of anti-H3 (abcam ab1791), or 5µl per IP of anti-PolII (Sigma-Aldrich 8WG16) and 25µl Protein G Agarose beads. Beads were washed with Lysis Buffer, Lysis Buffer with 500 mM NaCl, wash buffer (10 mM Tris-HCl pH 8, 0.25 M LiCl, 0.5% NP-40, 0.5% (w/v) sodium deoxycholate,1 mM EDTA) and TE. Immunoprecipitated DNA was recovered by first boiling with Chelex-100 resin (BioRad) for 12 min, before incubating with Proteinase K (Roche) for 30 min at 55°C with shaking at 1000rpm. Quantification of enrichment was performed by qPCR using LightCycler 480 SYBR Green (Roche) and primers listed in Table S5. Relative enrichments were calculated as the ratio of product of interest to control product (*his3*$^{+}$) in IP over input. In all cases, histograms represent three biological replicates and error bars represent one S.D.

ChIP-seq

150ml of cells per IP were grown in YES to an OD_{595} of 0.8-1.0 and fixed in 1% formaldehyde for 15 min at room temperature. Cells were lysed in 650µl of 50mM Hepes-KOH pH7.5, 140mM NaCl, 1mM EDTA, 1% (v/v) Triton X-100, 0.1%(w/v) sodium deoxycholate, 1x PMSF, 1x yeast protease inhibitors (Roche) using a bead beater (Biospec products) for 4 x 2 min at 4°C. Sonication was performed in lysis buffer containing 0.2% SDS, using a Bioruptor Twin (Diagenode) for a total of 28 min (30 sec on/30 sec off on 'high' power). Samples were pre-cleared using 50µl Protein G Agarose beads, before lysates were incubated overnight at 4°C, with 3µl per IP of anti-H3K9me2 (mAb 5.1.1 [76]) or 6µl per IP of anti-H3 (abcam ab1791) and 75µl Protein G Agarose beads. Beads were washed twice each with Lysis Buffer, Lysis Buffer with 500 mM NaCl, wash buffer (10 mM Tris-HCl pH 8, 0.25 M LiCl, 0.5% NP-40, 0.5% (w/v) sodium deoxycholate,1 mM EDTA) and TE. Immunoprecipitated DNA was recovered by incubating beads with 1x Elution buffer (10mM Tris-HCl pH8.0, 300mM NaCl, 5mM EDTA, 1% SDS) or input sample with 1.5x Elution buffer (15mM Tris-HCl pH8.0, 450mM NaCl, 7.5mM EDTA, 1.5% SDS) at 65°C for at least 6 hours with shaking at 1000rpm. Samples were then treated with RNase A at 37°C for 1 hour, before incubation with Proteinase K at 55°C for 2 hours. Immunoprecipitated DNA was recovered using PCR purification columns (Qiagen). ChIP-Seq libraries were prepared using NEBNext Library Prep Master Mix Set (NEB) according to manufacturer's instructions, then pooled and sequenced paired-end on an Illumina HiSeq 4000. Bioinformatic analysis was carried out using the Galaxy server[63], Raw reads were filtered for quality and adapters using Trim Galore! (version 0.4.3.1) [64]. Trimmed reads were then aligned to the *S. japonicus* reference genome SJ5 (GCA_000149845.2) using bowtie2 (version 2.3.4.3) [71]. bamCompare (version 3.3.2.0.0) [69] was used to compute the ratio of the number of reads between IP and Input samples.

Genomic DNA isolation

Genomic DNA was extracted from 10ml of cells grown to early stationary phase. Cells were lysed in SPZ buffer (1.2M Sorbitol, 50mM sodium citrate, 50mM Na_2HPO_4, 40mM EDTA, 400µg/ml Zymolyase 100T (Amsbio), adjusted to pH 5.6) at 37°C, and genomic DNA extracted by adding 10% SDS/5M KOAc. DNA was precipitated using ispopropanol and contaminating RNA removed using RiboShredder™ RNase Blend (Epicentre). RNase was removed using an equal volume of phenol:chloroform:isoamyl alcohol (25:24:1), and DNA was reprecipitated with ethanol for 10 min at -80°C.

gDNA-Seq

For sequencing of genomic DNA, libraries were prepared using Illumina Nextera XT DNA Library Prep Kit according to manufacturer's instructions, then pooled and sequenced paired-

end on an Illumina NextSeq550. Bioinformatic analysis was carried out using the Galaxy server [63]. Raw reads were filtered for quality and adapters using Trim Galore! (version 0.4.3.1). SNPs were called using the Snippy package (version 4.5.0) [77] with *S. japonicus* SJ5 (GCA_000149845.2) as the reference genome.

Supplementary Table S1 – List of up- and down- regulated genes in *dcr1Δ vs *wild type* cells**

Table_S1_Up_Downregulated_Genes_RNA_Seq.xlsx

Supplementary Table S2 – Genomic coordinates of the retrotransposon elements Tj1-21

Table_S2_SJ5_TE_Coordinates_Tj1-22.xlsx

Supplementary Table S3 – *S. japonicus* strains used in this study

Genotype	Source	Strain Identifier
h⁻ mat-P2028 ura4-D3 ade6(sj)-domE	Niki Lab [78]	EHB2742 (NIG 5384)
h⁺ mat-2017 ura4-D3 ade6(sj)-domE	Niki Lab [79]	EHB2743 (NIG5386)
h⁻ mat-P2028 dcr1Δ (dcr1^{dis}::natMX6 mpe1^{R77W}) ura4-D3 ade6(sj)-domE*	This Study	EHB3054
h⁻ mat-P2028 dcr1Δ† (dcr1^{del}::natMX6 leo1^{V61Stop}) ura4-D3 ade6(sj)-domE	This Study	EHB7518
h⁻ mat-P2028 tri1::ura4 ura4-D3 ade6(sj)-domE	This Study	EHB3369
h⁺ mat-2017 tri1::ura4 ura4-D3 ade6(sj)-domE	This Study	EHB3371
h⁻ mat-P2028 pku70::ura4 ura4-D3 ade6(sj)-domE	This Study	EHB3254
h⁺ mat-2017 pku70::ura4 ura4-D3 ade6(sj)-domE	This Study	EHB3256
h⁻ mat-P2028 pku80::ura4 ura4-D3 ade6(sj)-domE	This Study	EHB3258
h⁺ mat-2017 pku80::ura4 ura4-D3 ade6(sj)-domE	This Study	EHB3260
h⁻ mat-P2028 nmt1::ago1 ago1::NatMX6 ura4-D3 ade6(sj)-domE	This Study	EHB4652
h⁺ mat-2017 nmt1::clr4 clr4::NatMX6 ura4-D3 ade6(sj)-domE	This Study	EHB4732
h⁺ mat-2017 nmt1::dcr1 dcr1^{dis}::NatMX6 ura4-D3 ade6(sj)-domE	This Study	EHB5591
h⁺ mat-2017 nmt1::dcr1 dcr1^{del}::NatMX6 ura4-D3 ade6(sj)-domE	This Study	EHB5597
h⁻ mat-P2028 kanMX6-P3nmt1-3FLAG-ago1 ura4-D3 ade6(sj)-domE	This Study	EHB4279
h⁺ mat-2017 kanMX6-P3nmt1-3FLAG-ago1 ura4-D3 ade6(sj)-domE	This Study	EHB4282
h⁺ mat-2017 chp1-GFP-ura4 ura4-D3 ade6(sj)-domE	This Study	EHB2668
h⁺ mat-2017 rik1-FLAG-NatMX6 ura4-D3 ade6(sj)-domE	This Study	EHB2666
h⁺ mat-2017 stc1-GFP-ura4 ura4-D3 ade6(sj)-domE	This Study	EHB2670

h⁺ mat-2017 leo1::ura4 ura4-D3 ade6(sj)-domE	This Study	EHB5736
h⁺ mat-2017 leo1::ura4 dcr1^{del}::NatMX6 ura4-D3 ade6(sj)-domE	This Study	EHB7526
h⁺ mat-2017 leo1::ura4 ago1::NatMX6 ura4-D3 ade6(sj)-domE	This Study	EHB7549

Supplementary Table S4 – Plasmids used in this study

Plasmid	Source	Plasmid Identifier
pFA6a-natMX6	Carr Lab [80]	Euroscarf plasmid #P30437
pFA6a-*ago1Δ-natMX6*	This Study	N/A
pFA6a-*clr4Δ-natMX6*	This Study	N/A
pFA6a-*dcr1Δ^{dis}-natMX6*	This Study	N/A
pFA6a-*dcr1Δ^{del}-natMX6*	This Study	N/A
pREP1	Maundrell Lab [81]	N/A
pREP1SJ	This Study	N/A
pREP1SJ-*ago1⁺*	This Study	N/A
pREP1SJ-*clr4⁺*	This Study	N/A
pREP1SJ-*dcr1⁺*	This Study	N/A
pSO729	Oliferenko Lab [59]	N/A
pSO729-*chp1⁺-GFP-ura4^{sj+}*	This Study	N/A
pSO729-stc*1⁺*- GFP-*ura4^{sj+}*	This Study	N/A
pFA6a-5FLAG-*natMX6*	Noguchi Lab [60]	Addgene plasmid #19343
pFA6a-*rik1⁺*-5FLAG-*natMX6*	This Study	N/A
pFA6a-*kanMX6*-P3nmt1-3FLAG	Noguchi Lab [60]	Addgene plasmid #19336

Supplementary Table S5 – Oligonucleotides used in this study

Oligonucleotide Name	Oligonucleotide Sequence	Usage
q_Tj1_F	TATTATTGTGCCGAGCGAAGG	qPCR
q_Tj1_R	GATGACCACCGTTCACTGAG	qPCR
q_Tj2_F	GGAGACAATCCCGTTGGCTA	qPCR
q_Tj2_R	ACTGGATGTCCGGGTCAAAC	qPCR
q_Tj3_F	AACCGTCCACATCGCCGTAT	qPCR
q_Tj3_R	CGGTCCAGCAACTCGTCAAT	qPCR
q_Tj4_F	GGTACCACCAGAGGGTGAAC	qPCR
q_Tj5_F	GCAGTGTTCAAGCGTCTTCGG	qPCR
q_Tj5_R	GGAAGTTGACGCGCTTCCTG	qPCR
q_Tj6_F	GAGCAAAGGAGTGGCAGAGT	qPCR
q_Tj6_R	TTCGTCTGCGGTCTGTAACC	qPCR
q_Tj7_F	AAGAACCGATACGCGCTGC	qPCR
q_Tj7_R	CTTGCTGAAGACGCGTGC	qPCR
q_Tj8_F	AGCCGTCGAATTCGCCCTA	qPCR
q_Tj8_R	TTGAGGCCGCGGTAGTCAAT	qPCR
q_Tj9_F	AACGGGCGATGAGGAAACAA	qPCR
q_Tj9_R	TTCCGTCGCTGAGGTCTTCC	qPCR
q_Tj10_F	CATTCGGACTCACCAATGCG	qPCR

q_Tj10_R	TGTTGATCGCGGTCCTTTGA	qPCR
q_his3_F	TACAGACCCTAAAATTGCCC	qPCR
q_his3_R	CAAGCTTGGACGTAGGATTA	qPCR
Tj1A	GTTTGCCGCACTTCAACCCGAAA	Northern blot probe
Tj1B	CGCGTTCTTCTGTCAACTCCTGCG	Northern blot probe
Tj1C	TGAGGCCGTTCAGTCATTCTTGC	Northern blot probe
Tj2A	ACCGTTGTTCTTCGTTATCCTTA	Northern blot probe
Tj2B	CCGTCCTCGTCTCCGTGCCA	Northern blot probe
Tj2C	CCGTCCTGTTCGTTCGAAAGAA	Northern blot probe
Tj3A	TCAGGTGTTCGTCTTCCGTCTCTG	Northern blot probe
Tj3B	TAACTCGTTCAGCTGTCGGTCCA	Northern blot probe
Tj3C	TTGAACCGTCCACATCGCCGTA	Northern blot probe
Tj4A	ATGCCTTCTCCACATTCCGGACA	Northern blot probe
Tj4B	GCGTTCTGTATTGTTCTTCATA	Northern blot probe
Tj4C	CTCGTCTTGTTCCGTCCGACATGT	Northern blot probe
Tj5A	TGGCGCTCCAGTTCTGTTCGTTCG	Northern blot probe
Tj5B	TTTGCGTTTTCGCTCGCGTCCGTA	Northern blot probe
Tj5C	CAGCTGTCGTCGTCCTCCGTGTA	Northern blot probe
Tj6A	CTCCATTGTTCTTTCTTCCGCTT	Northern blot probe
Tj6B	TCTCCAAAGCCGTCTGCCCGCAA	Northern blot probe
Tj6C	GATACCACTGCTTCGCGTCCATGT	Northern blot probe
Tj7A	CGCTTGCTTGCTCCACGTCCGCG	Northern blot probe
Tj7B	TGATGACAAGAACGACGGCGTCACC	Northern blot probe
Tj7C	GATCGTTCTCTCGCTCTGCCCATC	Northern blot probe
Tj8A	CGCCGCGCCCAGCCCTACGTCA	Northern blot probe
Tj8B	CATGTCAGTCGTTCTTCGTCGTCGA	Northern blot probe
Tj8C	ACTACCGTCCTTCTTCCTCACGAA	Northern blot probe
Tj9A	TACCGCTCCACTGTGCCCGAGTC	Northern blot probe
Tj9B	ATCGCGTCTTCCAATCCTCGTT	Northern blot probe
Tj9C	ATCGTCCGTTCAGACTGTCCGT	Northern blot probe
Tj10A	CACCGTTTTGTCCAGATCTTCA	Northern blot probe
Tj10B	TCGCTCCACTTGCATTTGTCCG	Northern blot probe
Tj10C	GCTTTGCTCGTCTAGTCCGCAA	Northern blot probe
jap_snoRNA58	CTGCTAAATCAGAAGTCTAGCATC	Northern blot probe

A

Gene Target	Base strain	% Knockout
ago1⁺	*wild type*	0.00
clr4⁺	*wild type*	0.00
dcr1⁺	*wild type*	1.39
ago1⁺	*ectopic ago1⁺*	90.00
clr4⁺	*ectopic clr4⁺*	90.00
dcr1⁺	*ectopic dcr1⁺*	95.24

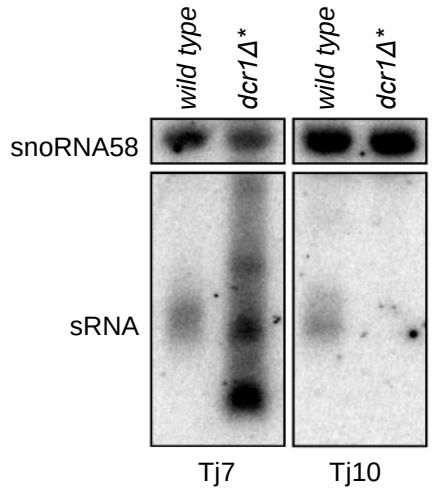

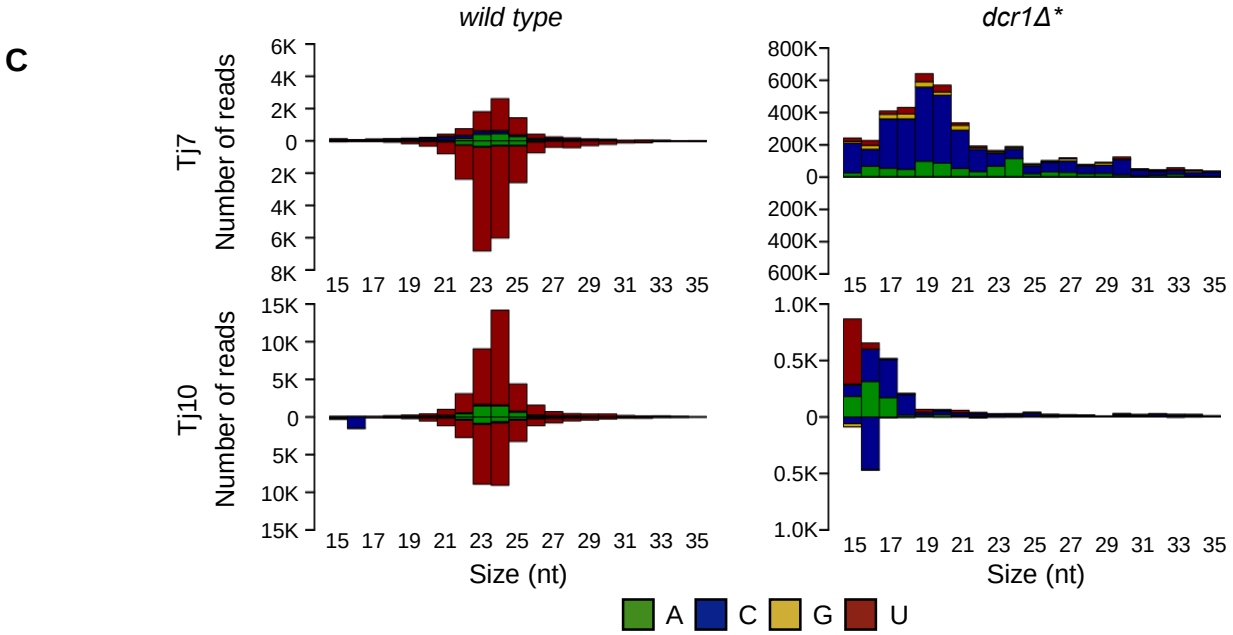

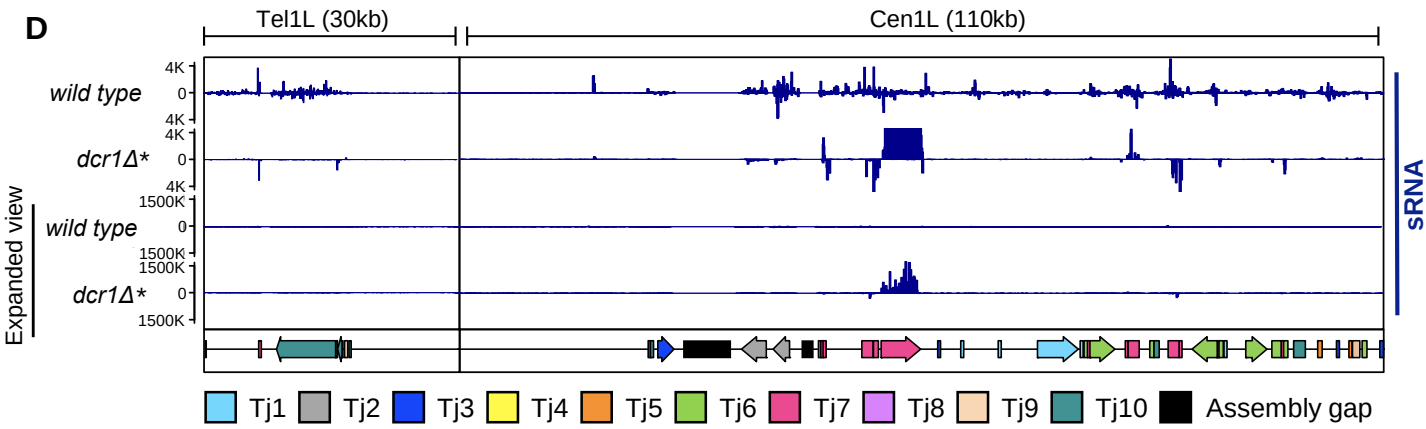

Figure 1. A functional RNAi pathway is required for viability in *S. japonicus*

(A) Knockout recovery rates of core RNAi and heterochromatin factors in *wild type* and ectopic expression backgrounds.

(B) Northern blot analysis of small RNA species isolated from wild type and *dcr1Δ** strains, probed with ^{32}P end-labelled oligonucleotides, antisense to the indicated retrotransposon or snoRNA58 loading control.

(C) Size profile, strand bias and 5' nucleotide preference of small RNA species that map to indicated retrotransposons, isolated from wild type and *dcr1Δ** strains. RNAs derived from the sense strand are plotted above the axis, whilst RNAs derived from the antisense strand are plotted below.

(D) Genome view of mapped small RNA species at two retrotransposon-rich loci, in wild type and *dcr1Δ** backgrounds. Note differing scale in the expanded view tracks. The positions of individual transposable elements are indicated by coloured arrows below the data track.

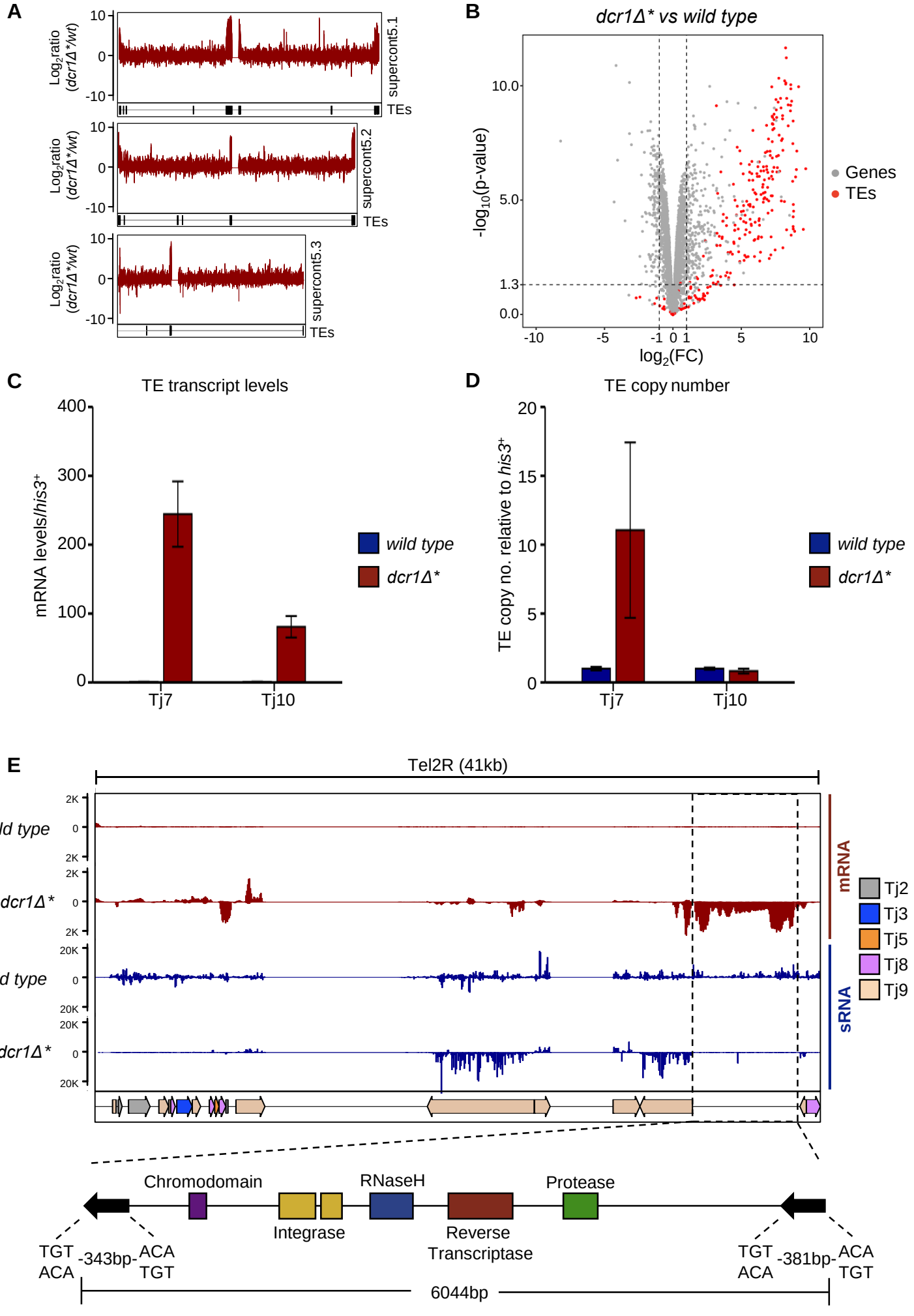
A
Log2ratio (dcr1Δ*/wt)
supercont5.1
supercont5.2
supercont5.3
TEs
B
dcr1Δ* vs wild type
-log10(p-value)
log2(FC)
Genes
TEs
C
TE transcript levels
mRNA levels/his3+
wild type
dcr1Δ*
Tj7
Tj10
D
TE copy number
TE copy no. relative to his3+
E
Tel2R (41kb)
wild type
dcr1Δ*
mRNA
sRNA
Tj2
Tj3
Tj5
Tj8
Tj9
Chromodomain
RNaseH
Protease
Integrase
Reverse Transcriptase
TGT ACA
-343bp-
ACA TGT
-381bp-
6044bp

Figure 2. Rare *dcr1Δ* survivors exhibit activation of transposable elements.

(A) Ratio of mapped RNA-Seq reads in *dcr1Δ** vs *wild type* cells for the three main chromosomal contigs of the SJ5 annotation. TE locations are indicated by black bars underneath each data track.

(B) Volcano plot of differentially expressed genes from RNA-Seq in *dcr1Δ** vs *wild type* cells. Differentially expressed retrotransposons are indicated in red, with all other genes in grey. Dotted lines indicate a –log10(p-value) of ~1.3 (equivalent to p = 0.05) and -1 > Log2FC > 1 (indicating a 2-fold change in expression in mutant vs wild type).

(C) RT-qPCR analysis of retrotransposon transcript levels, relative to *his3*$^{+}$, normalised to wild type. Data plotted are the mean ± SD from three replicates.

(D) qPCR analysis of retrotransposon copy number, relative to *his3*$^{+}$, normalised to wild type. Data plotted are the mean ± SD from three replicates.

(E) Example of a novel TE locus discovered from analysis of siRNA and mRNA-seq data. Regions that displayed loss of small RNAs and gain of mRNA signal in the *dcr1Δ* mutant vs *wild type* were searched for known retrotransposon protein motifs using the NCBI domain search tool. These sequences were then searched against the rest of the SJ5 genome sequence using BLAST to identify the location of other TE copies. The positions of individual transposable elements are indicated by coloured arrows below the data track.

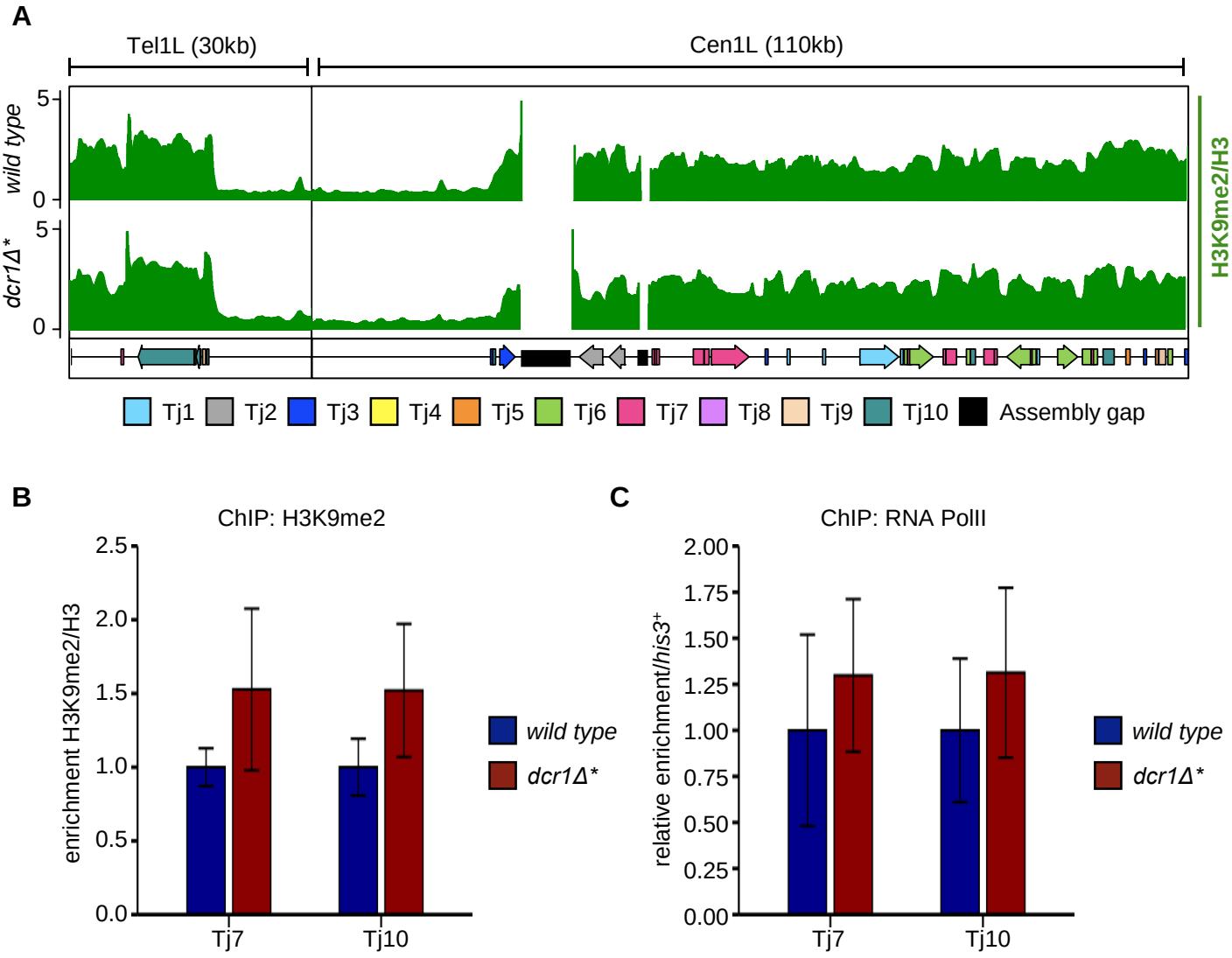

Figure 3. Levels of H3K9 methylation and transcription at retrotransposon loci are unaffected in rare *dcr1Δ* survivors

(A) ChIP-seq profile of H3K9me2 across two retrotransposon-rich loci in *wild type* and *dcr1Δ** cells. The positions of individual transposable elements are indicated by coloured arrows below the data track.

(B) ChIP-qPCR analysis of H3K9me2/H3 levels at Tj7 and Tj10 retroelements, normalised to wild type. Data plotted are the mean ± SD from three replicates.

(C) ChIP-qPCR analysis of RNA PolII levels at at Tj7 and Tj10 retroelements, relative to *his3*$^{+}$, normalised to wild type. Data plotted are the mean ± SD from three replicates.

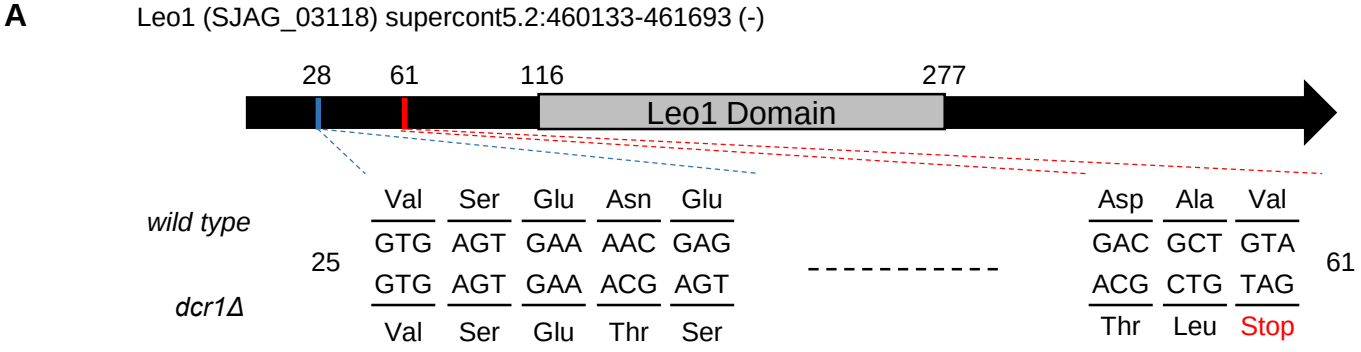

B

Gene Target	Base strain	% Knockout
dcr1⁺	*wild type*	1.39
ago1⁺	*wild type*	0.00
clr4⁺	*wild type*	0.00
dcr1⁺	*leo1Δ*	79.17
ago1⁺	*leo1Δ*	63.33
clr4⁺	*leo1Δ*	0.00

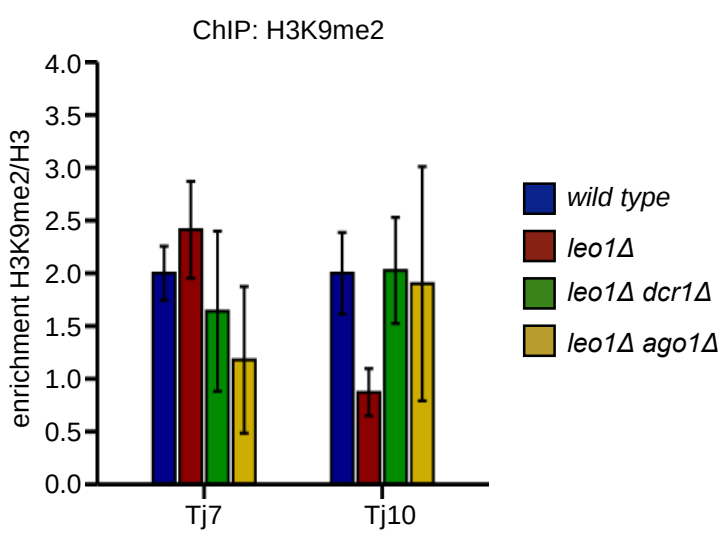

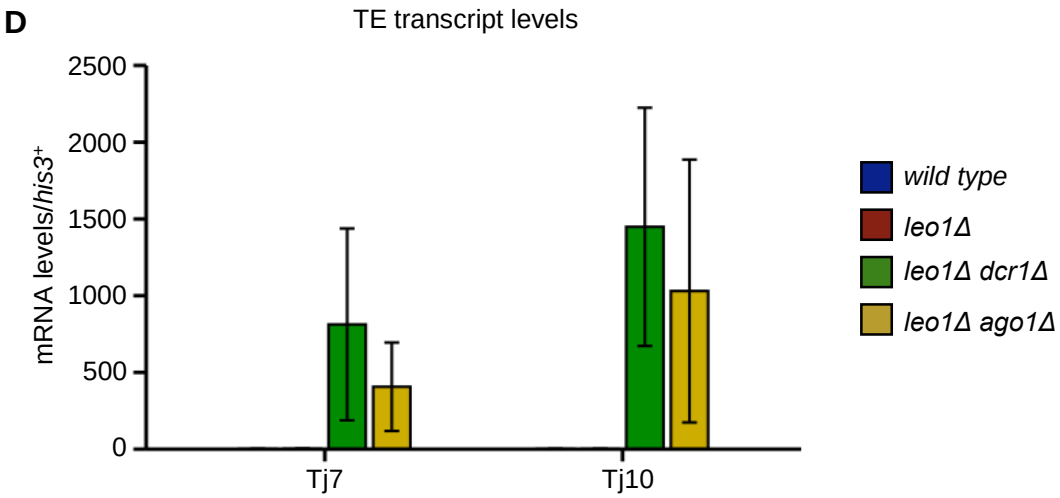

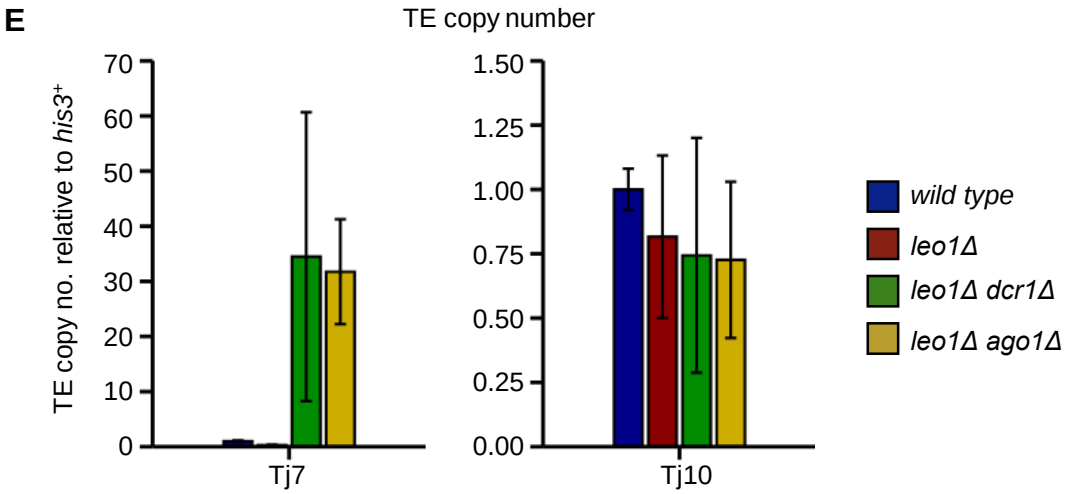

Figure 4. Mutation of the Paf1 complex subunit Leo1 facilitates survival of RNAi mutants.

(A) Schematic showing the location of the sequenced mutation within Leo1. The single base pair deletion causes a frameshift, which leads to the introduction of a premature stop codon after 61 amino acids.

(B) Knockout recovery rates of core RNAi and heterochromatin factors in *wild type* and *leo1Δ* backgrounds.

(C) ChIP-qPCR analysis of H3K9me2/H3 levels at Tj7 and Tj10 retroelements, normalised to wild type. Data plotted are the mean ± SD from three replicates.

(D) RT-qPCR analysis of retrotransposon transcript levels, relative to *his3*$^{+}$, normalised to wild type. Data plotted are the mean ± SD from three replicates.

(E) qPCR analysis of retrotransposon copy number, relative to *his3*$^{+}$, normalised to wild type. Data plotted are the mean ± SD from three replicates.

Gene Target	Gene ID	Base Strain	Genetic manipulation	Resistant colonies screened	Colonies positive by PCR	% Correct
arb1^{+}	SJAG_02594	*wild type*	deletion	16	0	0.00
arb2^{+}	SJAG_04061	*wild type*	deletion	16	0	0.00
ago1^{+}	SJAG_02621	*wild type*	deletion	119	0	0.00
chp1^{+}	SJAG_03916	*wild type*	deletion	27	0	0.00
dcr1^{+}	SJAG_03689	*wild type*	deletion	144	2	1.39
rdp1^{+}	SJAG_03356	*wild type*	deletion	16	0	0.00
clr4^{+}	SJAG_04574	*wild type*	deletion	54	0	0.00
rik1^{+}	SJAG_03680	*wild type*	deletion	31	0	0.00
stc1^{+}	SJAG_02409	*wild type*	deletion	27	0	0.00
tri1^{+}	SJAG_01836	*wild type*	deletion	16	12	75.00
pku70^{+}	SJAG_05372	*wild type*	deletion	10	9	90.00
pku80^{+}	SJAG_04372	*wild type*	deletion	10	8	80.00
ago1^{+}	SJAG_02621	*ectopic ago1*$^{+}$	deletion	10	9	90.00
clr4^{+}	SJAG_04574	*ectopic clr4*$^{+}$	deletion	10	9	90.00
dcr1^{+}	SJAG_03689	*ectopic dcr1*$^{+}$	deletion	42	40	95.24
ago1^{+}	SJAG_02621	*wild type*	N-terminal 3xFLAG	14	6	42.86
chp1^{+}	SJAG_03916	*wild type*	C-terminal GFP	12	9	75.00
rik1^{+}	SJAG_03680	*wild type*	C-terminal 3xFLAG	4	4	100.00
stc1^{+}	SJAG_02409	*wild type*	C-terminal GFP	6	5	83.33

Figure S1. Core RNAi and heterochromatin factors cannot be deleted without the presence of an ectopic copy, but they can be epitope tagged

Knockout and tagging rates of targeted genes in either the wild type background, or in the presence of an ectopic gene copy.

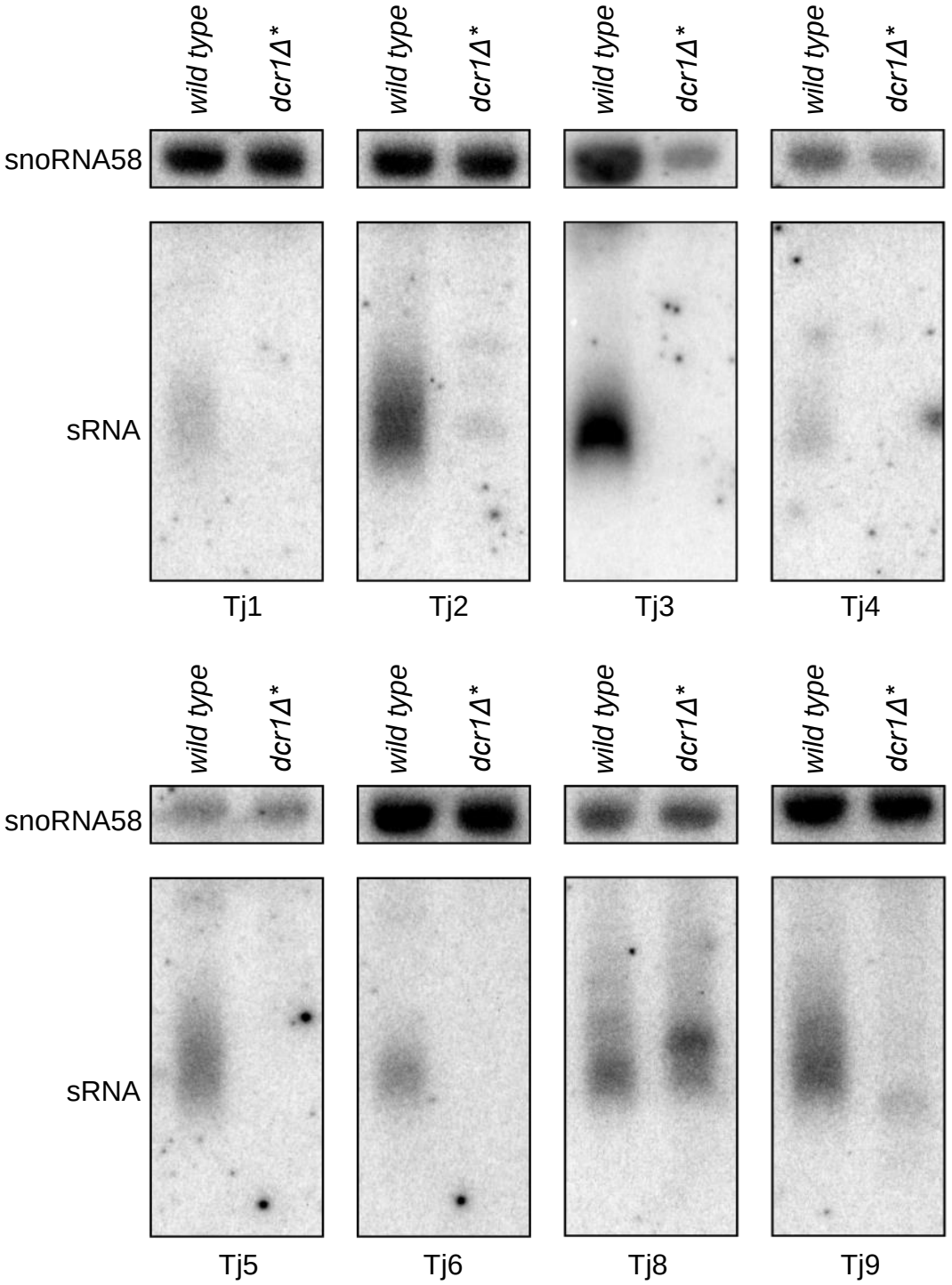

Figure S2. Deletion of Dcr1 abolishes siRNA production, however specific transposable elements give rise to alternative small RNA species

Northern blot of small RNA species isolated from wild type and *dcr1Δ** strains, probed with ^{32}P end-labelled oligonucleotides, antisense to the indicated retrotransposon or snoRNA58, a loading control.

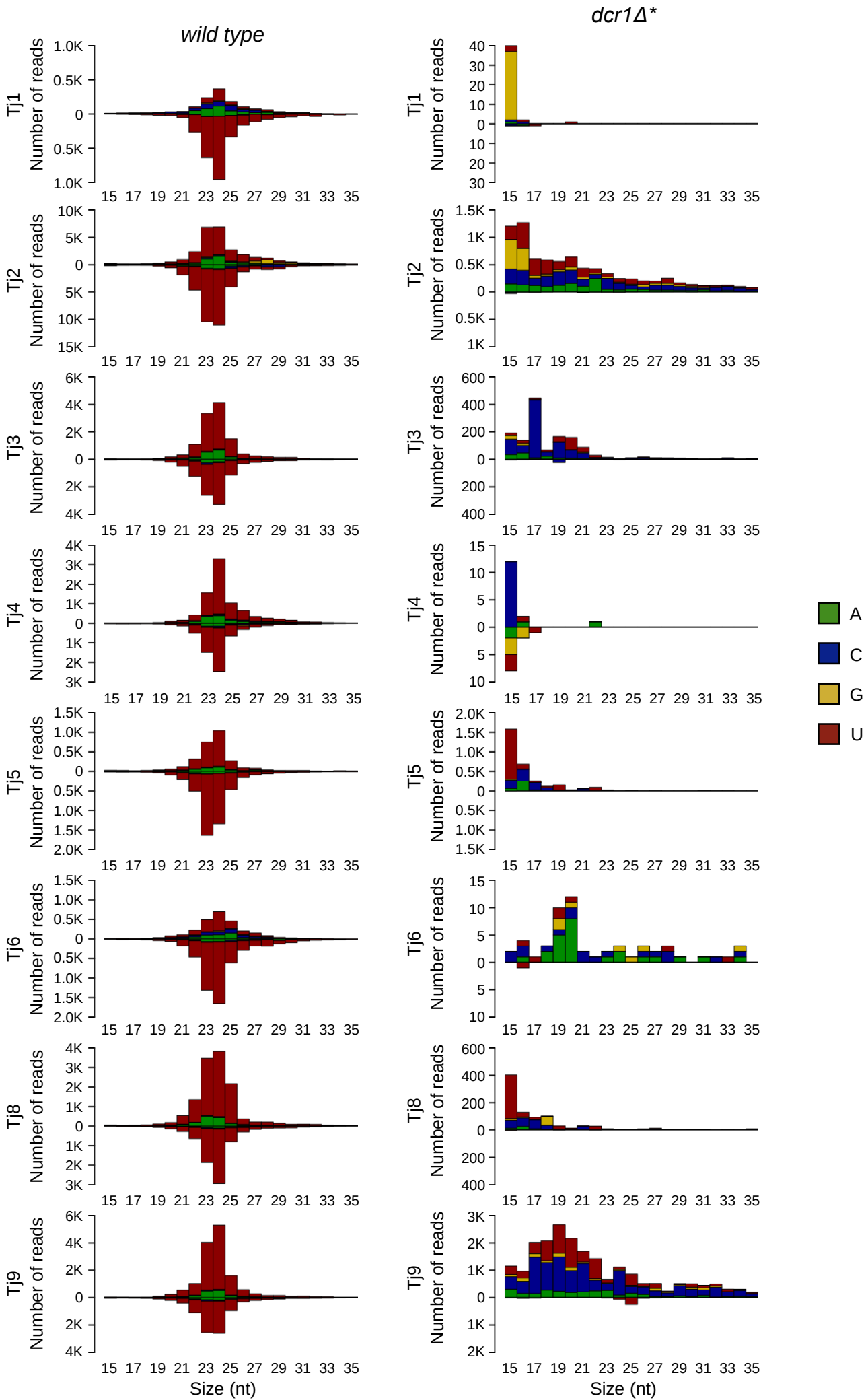
wild type
dcr1Δ*
Tj1
Tj2
Tj3
Tj4
Tj5
Tj6
Tj8
Tj9
Number of reads
Size (nt)
A
C
G
U

Figure S3. TE derived small RNA species present in the *dcr1Δ background lack the characteristics of siRNAs**

Size profile, strand bias and 5’ nucleotide preference of small RNA species that map to indicated retrotransposons, isolated from wild type and *dcr1Δ** strains. RNAs derived from the sense strand are plotted above the axis, whilst RNAs derived from the antisense strand are plotted below.

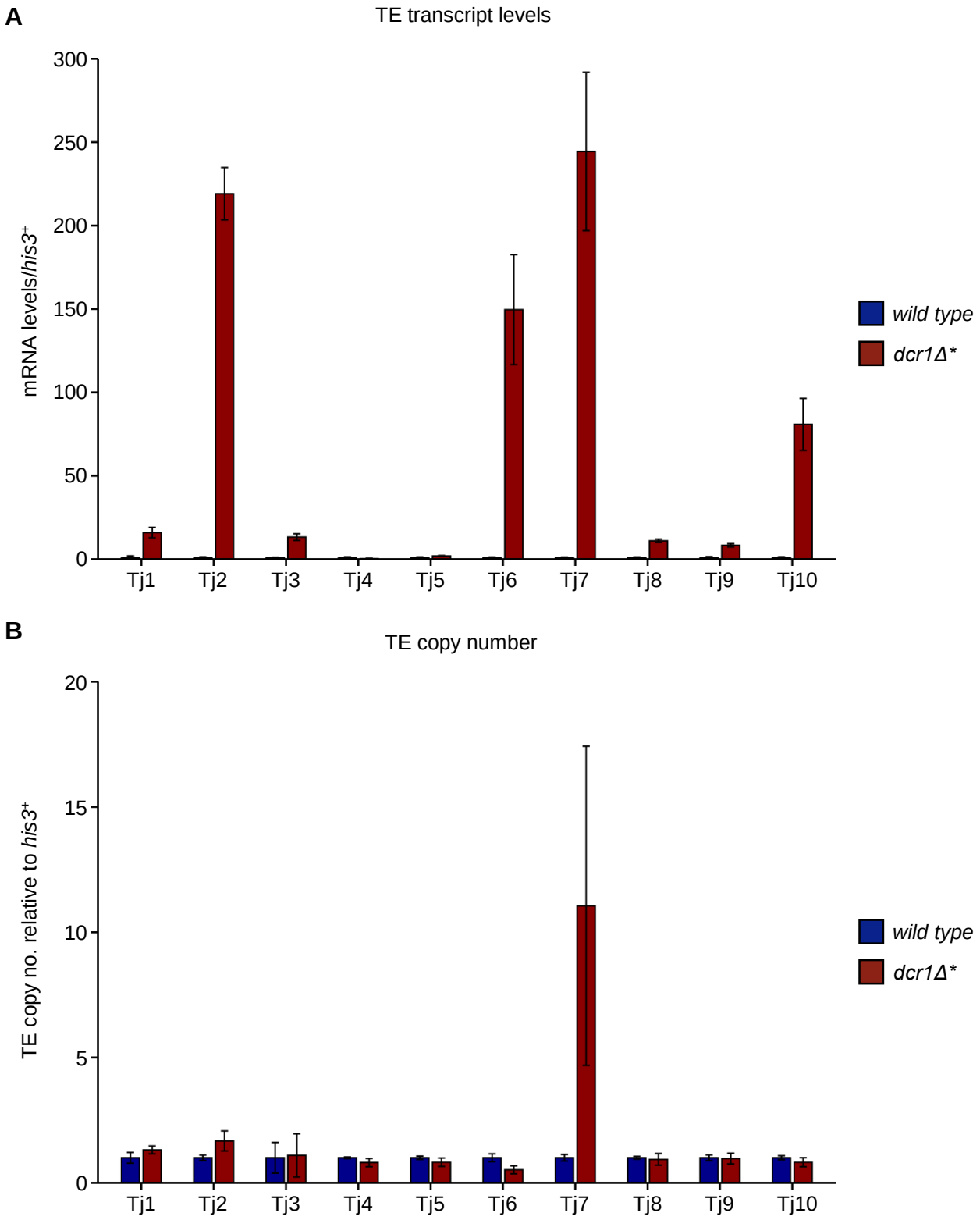

Figure S4. Absence of Dcr1 is associated with accumulation of retrotransposon transcript for a majority of TE families, but mobilisation of only Tj7

(A) RT-qPCR analysis of retrotransposon transcript levels, relative to *his3*$^{+}$, normalised to wild type. Data plotted are the mean ± SD from three replicates.

(B) qPCR analysis of retrotransposon copy number, relative to *his3*$^{+}$, normalised to wild type. Data plotted are the mean ± SD from three replicates.

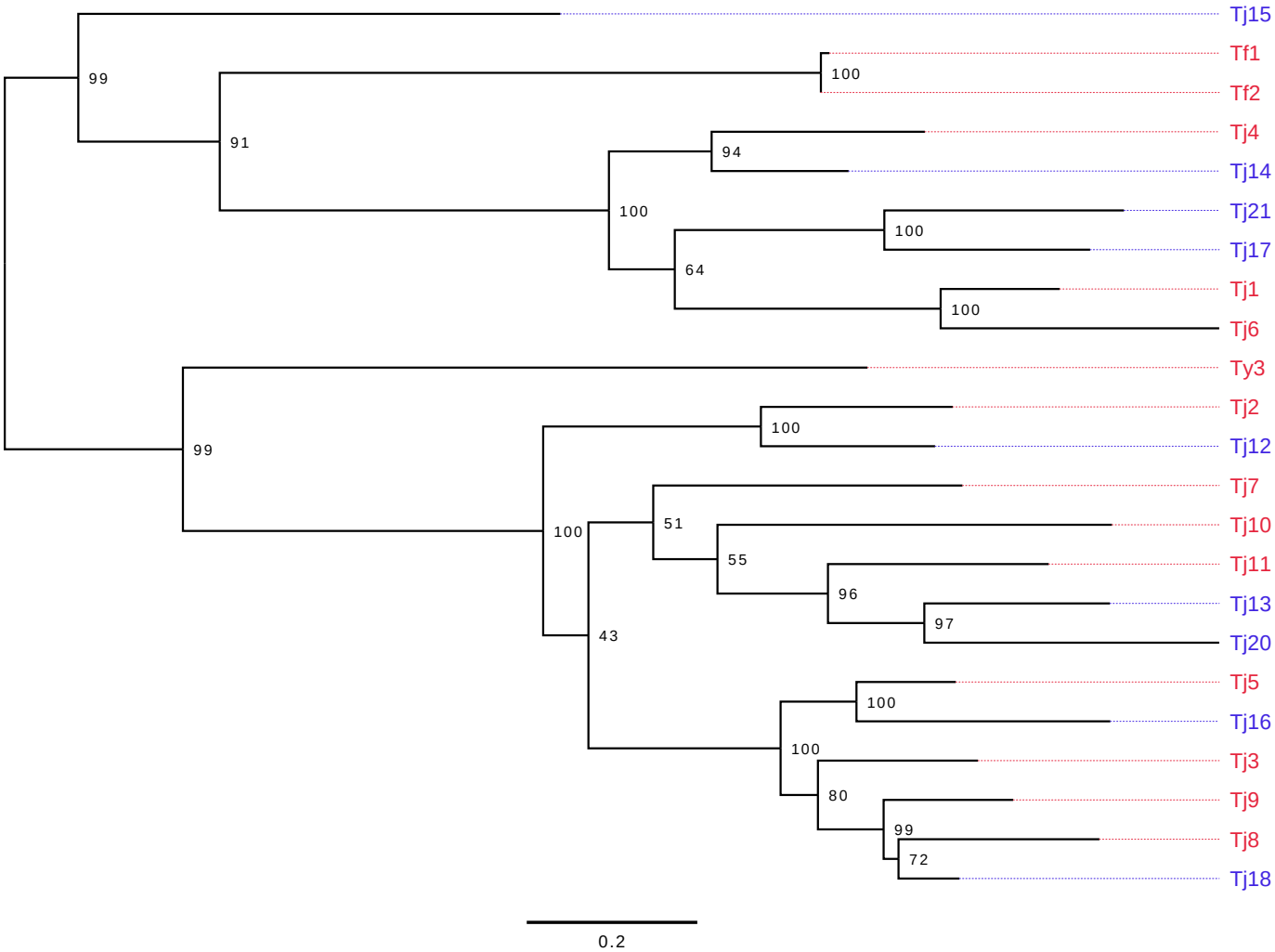

Figure S5. Three loci phylogenetic analysis of newly discovered retrotransposons indicates that these are novel elements that fall into the two existing lineages *of S. japonicus* retroelements
For each newly discovered retrotransposon, the sequences of the reverse transcriptase, RNase and integrase domains were aligned to the corresponding domains from Tj1-10, as well as *S. pombe* Tf1 and Tf2 and *S. cerevisiae* Ty3 using ClustalW. IQtree2 was then used to build a single tree based on the three loci, with 1000 ultrafast bootstraps. IQtree2 selected TVM+F+R3 as the best-fitting base substitution model using the Bayesian Information Criterion (BIC). Node labels indicate bootstrapping values. Scale bar is in units of base substitutions per site. Retrotransposons discovered in this study are highlighted in blue, previously discovered retrotransposons are highlighted in red.

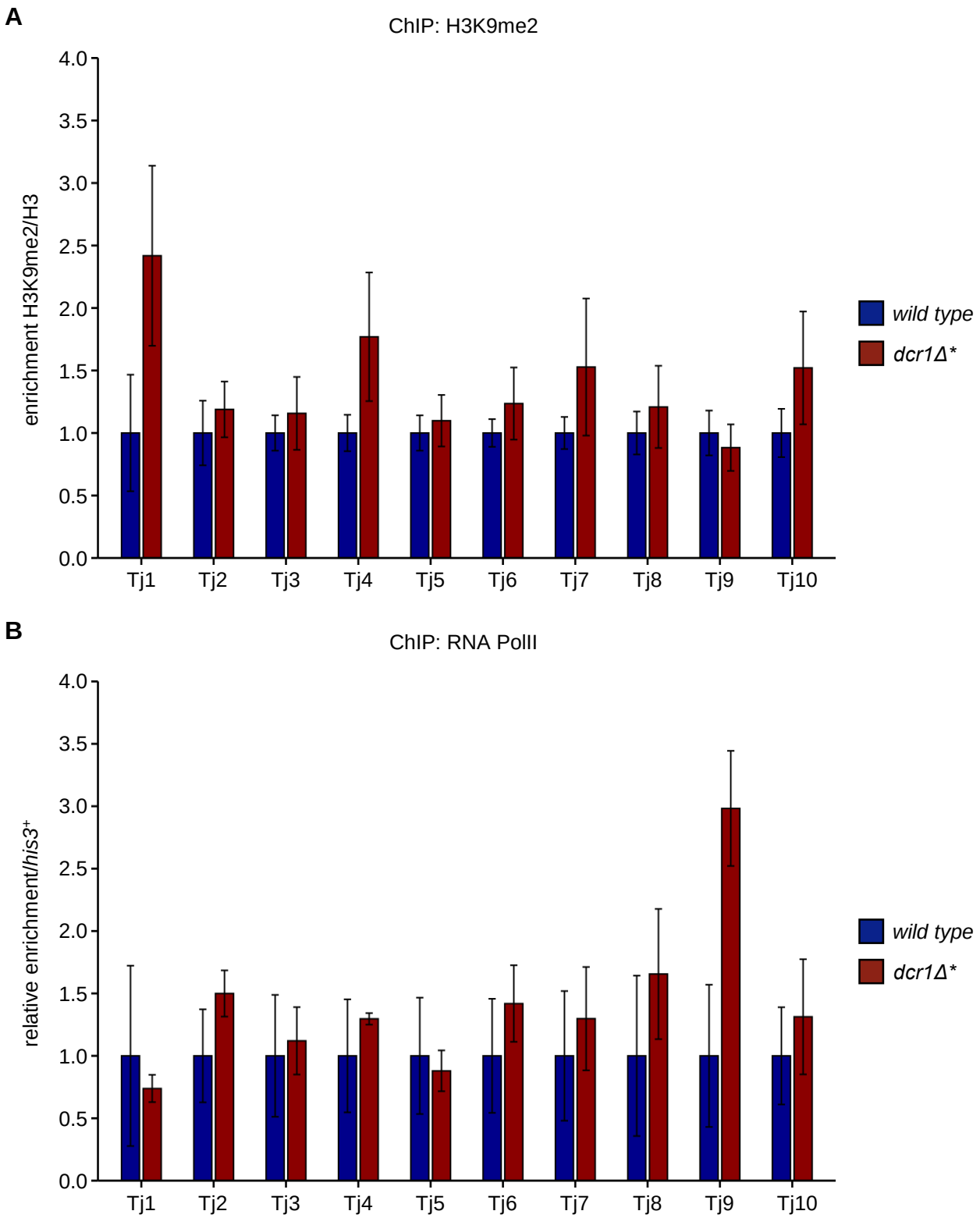

Figure S6. H3K9me2 levels and RNA PolII occupancy at retrotransposons are unchanged in the absence of Dcr1

(A) ChIP-qPCR analysis of H3K9me2/H3 levels across retrotransposons, normalised to wild type. Data plotted are the mean ± SD from three replicates.

(B) ChIP-qPCR analysis of RNA PolII levels across retrotransposons, relative to *his3*$^{+}$, normalised to wild type. Data plotted are the mean ± SD from three replicates.

A

Chromosome	*Position*	*Type*	*Reference*	*Alternate*	*Strand*	*Nucleotide Position*	*Amino Acid Position*	*Effect*	*Gene ID*	*Gene Name*	*Product*	*Notes*
supercont5.1	1214961	SNP	G	A	-	229/1467	77/488	R77W	SJAG_02668	*mpe1*	ubiquitin-protein ligase E3 RBBP6 family protein	R77W mutation in DWNN of Mpe1

B

Chromosome	*Position*	*Type*	*Reference*	*Alternate*	*Strand*	*Nucleotide Position*	*Amino Acid Position*	*Effect*	*Gene ID*	*Gene Name*	*Product*	*Notes*
supercont5.1	4064349	SNP	T	C	-	773/1350	258/449	T258C	SJAG_00099	*N/A*	Delta(12) fatty acid desaturase	Causes Y258C mutation in FA_desaturase domain - unconserved residue
supercont5.2	461549	Deletion	GT	G	-	83/1297	28/431	N28 frameshift	SJAG_03118	*leo1*	RNA polymerase II associated Paf1 complex	Causes premature stop after 60aa in Leo1
supercont5.2	991551	Deletion	AT	A	-	3824/3906	1275/1301	N1275 frameshift	SJAG_03384	*wis4*	STE/STE11 protein kinase	Causes readthrough transcription and addition of 38aa to end of protein
supercont5.5	44842	SNP	A	G	-	12/805	4/267	F4F	SJAG_05143	*N/A*	hypothetical protein	Retrotransposon gag protein
supercont5.6	47743	Insertion	C	CTT	+	2681/5945	894/1980	R894 frameshift	SJAG_05105	*tlh1/2*	hypothetical protein	RecQ type DNA helicase

Figure S7. Rare *dcr1Δ* survivors carry potential compensatory mutations that facilitate their survival

(A) Table of SNPs within coding regions sequenced from the *dcr1Δ** strain

(B) Table of SNPs within coding regions sequenced from the *dcr1Δ†* strain

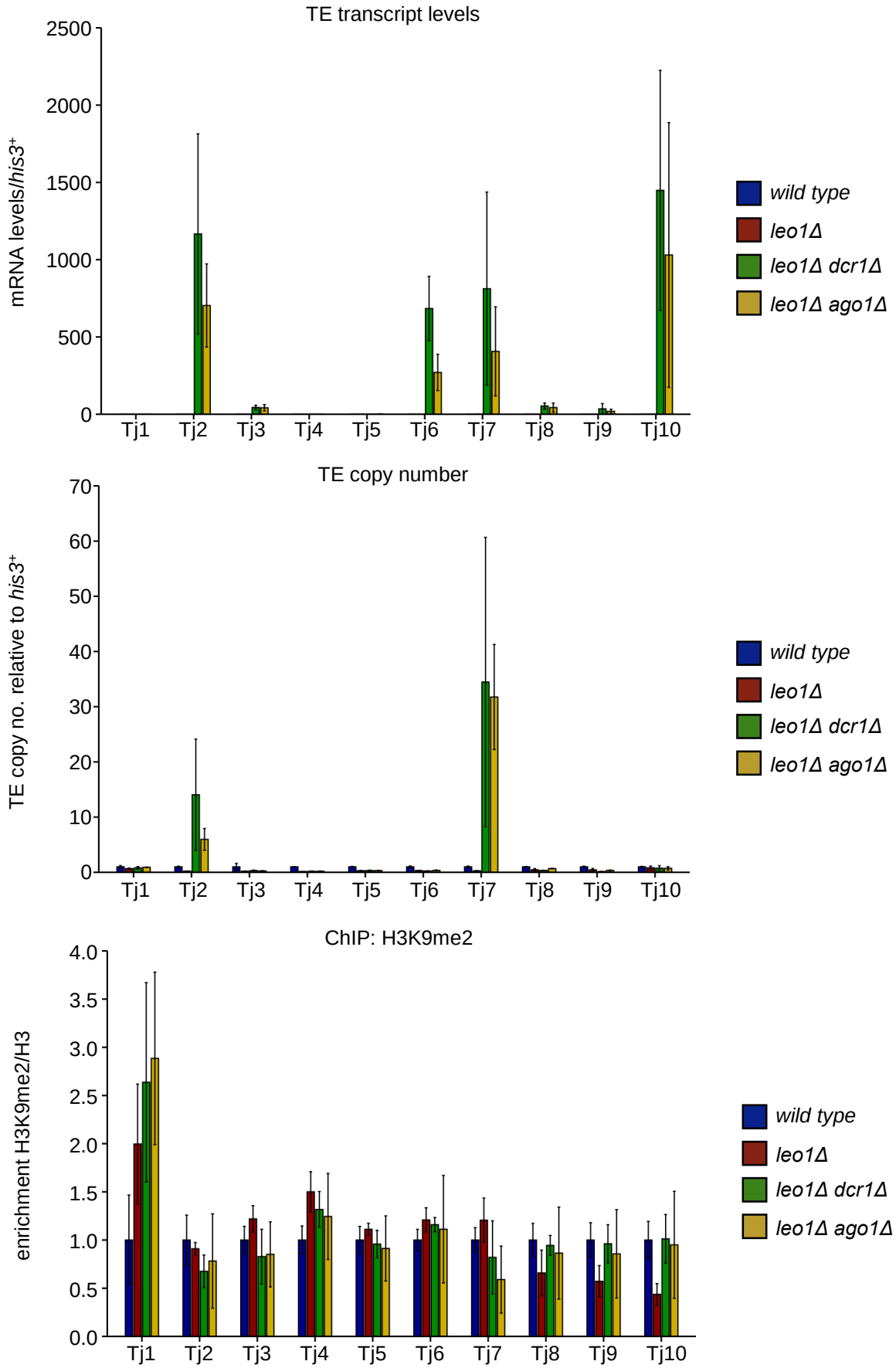

Figure S8. *leo1Δ dcr1Δ and leo1Δ ago1Δ* strains show similar activation of retrotransposons independent of H3K9 methylation

(A) RT-qPCR analysis of retrotransposon transcript levels, relative to *his3*$^{+}$, normalised to wild type. Data plotted are the mean ± SD from three replicates.

(B) qPCR analysis of retrotransposon copy number, relative to *his3*$^{+}$, normalised to wild type. Data plotted are the mean ± SD from three replicates.

(C) ChIP-qPCR analysis of H3K9me2/H3 levels across retrotransposons, normalised to wild type. Data plotted are the mean ± SD from three replicates.